Chapter 3
Principles of Virus Structural Organization

B.V. Venkataram Prasad and Michael F. Schmid

Abstract Viruses, the molecular nanomachines infecting hosts ranging from prokaryotes to eukaryotes, come in different sizes, shapes, and symmetries. Questions such as what principles govern their structural organization, what factors guide their assembly, how these viruses integrate multifarious functions into one unique structure have enamored researchers for years. In the last five decades, following Caspar and Klug's elegant conceptualization of how viruses are constructed, high-resolution structural studies using X-ray crystallography and more recently cryo-EM techniques have provided a wealth of information on structures of a variety of viruses. These studies have significantly furthered our understanding of the principles that underlie structural organization in viruses. Such an understanding has practical impact in providing a rational basis for the design and development of antiviral strategies. In this chapter, we review principles underlying capsid formation in a variety of viruses, emphasizing the recent developments along with some historical perspective.

3.1 Introduction

Viruses are metastable macromolecular assemblies composed of the viral genome enclosed within a proteinaceous capsid. They come in variety of sizes, shapes, and forms. Some are large, and some are small; some are spherical, and some are rod-like; some have lipid envelopes. Many of these viruses exhibit exquisitely symmetric organization. Irrespective of their shape and size, the underlying theme in all these viruses is that the virus structure is designed to contain and protect the viral genome and deliver it to a specific host cell for subsequent replication of the virus. Viruses are also distinguished based on the type of the genome that they contain: single-stranded or double-stranded RNA or DNA. The viral genome, in addition to encoding the proteins that constitute the capsid, also encodes other proteins referred to as nonstructural proteins, so called because they are not part of the final capsid's organization. These nonstructural proteins are essential for viral replication inside the host cell. In some viruses, particularly of bacterial origin, viral genome encodes a protein called scaffolding protein that may not be part of the mature capsid but may be a critical factor in facilitating the capsid assembly.

B.V.V. Prasad (✉) • M.F. Schmid
Department of Biochemistry and Molecular Biology, Keck Center for Computational Biology,
Baylor College of Medicine, Houston, TX 77030, USA
e-mail: vprasad@bcm.tmc.edu

M.G. Rossmann and V.B. Rao (eds.), *Viral Molecular Machines*,
Advances in Experimental Medicine and Biology 726, DOI 10.1007/978-1-4614-0980-9_3,
© Springer Science+Business Media, LLC 2012

Often, the size of the virus is proportional to the size of the genome. However, the viral genome contributes far less to the total mass of the virion than the capsid proteins. It was this observation that prompted Watson and Crick to suggest that the capsid has to be formed by the association of multiple copies of the capsid protein(s) (Crick and Watson 1956, 1957). Such an assembly with repeating subunits then greatly reduces the amount of genetic information required. In some viruses, the capsid formation involves a single gene product, whereas in other viruses which are more complex, it involves multiple gene products. Such an assembly involving repeating subunits raises several interesting questions. How do these subunits interact with one another with high fidelity and specificity to form the capsid architecture? This question becomes even more interesting in complex viruses in which the capsid formation involves multiple gene products. Are there any specific structural properties that these proteins should have for the capsid formation? How is capsid assembly directed and controlled? How is the genome encapsidated? In addition to containing and protecting the genome, the capsid architecture must also be conducive for interactions with the host cell for entry; how is this process coordinated? Given that capsid has to disassemble to make the genome available for replication, what are the cues for disassembly? How does the capsid organization respond to and evade the antiviral response mounted by the host?

In the last half century, structural studies on a variety of viruses have provided a wealth of information regarding some of the questions listed above. In addition to providing insight into the fundamental principles underlying various aspects of capsid assembly, more importantly, such studies have had practical impact in providing a rational basis for the design and development of antiviral strategies. Several excellent reviews on virus structures and principles underlying capsid formation have been published periodically over years (Klug and Caspar 1960; Caspar and Klug 1962; Rossmann and Johnson 1989; Johnson and Speir 1997; Harrison 2007); we will emphasize here the recent developments along with the some historical perspective.

3.2 Structural Techniques

Two principal techniques used in the structural studies on viruses are electron microscopy and X-ray crystallography. Contributions from other elegant studies using a variety of biochemical and biophysical techniques and theoretical modeling have been crucial in providing a more complete understanding of the capsid construction and assembly pathways. Electron microscopy of negatively stained virus specimens provided the first glimpse of viruses and led to early classification of viruses based on shape and form (Green et al. 1956; Brenner and Horne 1959; Horne and Wildy 1962, 1979; Wildy and Horne 1963). Even today, this technique is used as a diagnostic tool in identifying clinical virus samples. Subsequently, the discovery that EM images of virus particles, which are essentially projection images, can be used to reconstruct the three-dimensional structure of the virus using computer image analysis protocols (Crowther et al. 1970) paved the way for spectacular advances in specimen preparation (Knapek and Dubochet 1980; Dubochet et al. 1988), electron imaging, and computer image reconstructions. In the last two decades, this exciting new technology called three-dimensional cryo-electron microscopy (cryo-EM) has revolutionized the structure analysis of a variety of viruses (Baker et al. 2010; Crowther 2010; Grigorieff and Harrison 2011).

Much of our understanding of subunit interactions in a viral capsid at the atomic level has come from X-ray crystallographic structure of spherical viruses. Beginning with the structures of three small spherical plant viruses in early 1980s (Harrison et al. 1978; Abad-Zapatero et al. 1980; Liljas et al. 1982), over the last three decades, X-ray crystallography has been successfully applied to study a variety of larger and more complex spherical viruses including human viruses (Hogle et al. 1985; Rossmann et al. 1985; Liddington et al. 1991; Grimes et al. 1998; Reinisch et al. 2000; Wikoff et al. 2000; Reddy et al. 2010). The closely related technique of X-ray fiber diffraction has

been used to study viruses that have helical symmetry (Namba and Stubbs 1986; Namba et al. 1989). In recent years, cryo-EM technique has allowed visualization of a variety of spherical viruses at subnanometer (Bottcher et al. 1997; Conway et al. 1997; Jiang et al. 2003; Zhang et al. 2003; Saban et al. 2006; Li et al. 2009) to near-atomic resolutions (Yu et al. 2008a, b; Baker et al. 2010; Liu et al. 2010; Wolf et al. 2010; Settembre et al. 2011, see also Chap. 4). For some viruses that are not amenable for high-resolution structural analysis by these techniques, complementarity between cryo-EM and X-ray crystallography has been exploited in deriving the pseudoatomic models of the capsid (Grimes et al. 1997; Mathieu et al. 2001; Zhang et al. 2002, 2007; Settembre et al. 2011). In these studies, when the virus capsid could not be crystallized, but a lower resolution structure could be determined by cryo-EM, as this technique does not require the specimen in a crystalline form, independently determined X-ray crystallographic structures of the capsid components are fitted into lower-resolution cryo-EM map of the capsid. Such a hybrid technique has been most useful in studying capsid–receptor, capsid–antibody interactions and in studying capsid-associated structural dynamics (Rossmann et al. 1994; Ilag et al. 1995; Smith et al. 1996; Stewart et al. 1997; Belnap et al. 2000; Conway et al. 2001; Martin et al. 2001; Nason et al. 2001; Dormitzer et al. 2004; Gan et al. 2006). Structure determination of spherical viruses either by X-ray crystallography or cryo-EM techniques relies implicitly on the symmetry of the capsid. As a result, the structural organization of the encapsidated genome is amenable to these structural techniques only when the genome follows the capsid symmetry. However, in recent years, there are several examples in which the entire genome or a significant portion of it is observed to follow the capsid symmetry and visualized in the structural analysis (Chen et al. 1989; Namba et al. 1989; Fisher and Johnson 1993; Larson et al. 1993). A detailed discussion on the genome organization in viruses is provided in a review by Prasad and Prevelige (2003). In this review, we mainly focus on the capsid organization. In addition to the X-ray crystallographic and cryo-EM structural techniques, other diffraction techniques such as neutron diffraction (Bentley et al. 1987), low-angle X-ray scattering (Tsuruta et al. 1998), and spectroscopic techniques (Tuma and Thomas 1997; Benevides et al. 2002) have been useful in understanding the capsid organization in viruses.

3.3 Capsid Organization in Spherical Viruses

3.3.1 Cubic Symmetry

It was Watson and Crick (1956) who first proposed that spherical viruses exhibit cubic symmetry involving at least four threefold rotational symmetry axes. They argued that only such symmetry in an isometric capsid allows close packing of repeating subunits such that each subunit has identical environment. The cubic symmetry is inherent in the platonic solids, the tetrahedron, cube, octahedron, dodecahedron, and icosahedron. The distinguishing characteristics of these polyhedral solids are that each polyhedron consists of identical faces, in the shape of a regular polygon; identical vertices, which are meeting points of the same number of faces; and identical edges, which are lines joining the adjacent vertices (Fig. 3.1). For example, a cube consists of six identical faces, each of which is a square; eight identical vertices, which are meeting points of three squares; and 24 edges, each joining adjacent vertices. These highly symmetric polyhedra can also be described in terms of the inherent rotational symmetry axes, wherein rotation of $360/n^\circ$ about an n-fold symmetry axis produces n invariant views of the polyhedron. For instance, a cube has twofold rotational symmetry axes passing through the centers of the opposite faces and threefold axes along the diagonals passing through each of the vertices. The combination of these two rotational symmetry elements gives rise to additional rotational symmetry axes: three fourfold symmetry axes going through centers of the

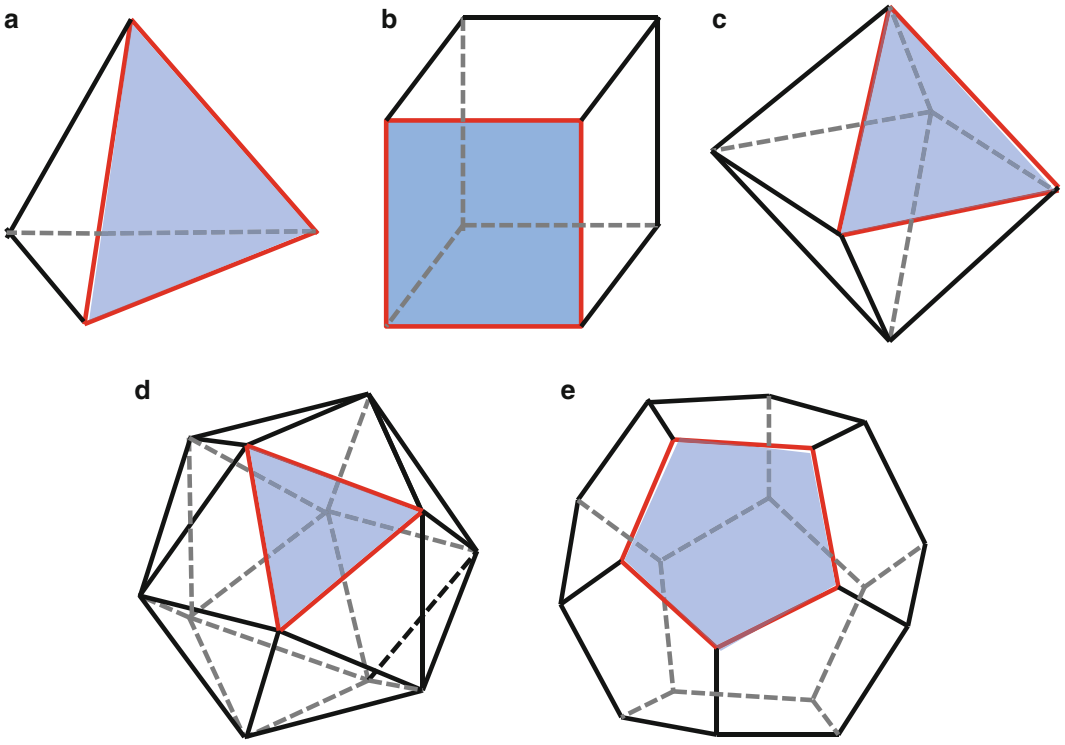


Fig. 3.1 The five platonic solids. One of the faces in each of these solids is colored in *pale blue*. The number of vertices (V), faces (F), and edges in each of these solids follows Euler formula, $F+V=E+2$. (**a**) Tetrahedron, which displays two- and threefold symmetry axes, has 4 triangular faces, 4 vertices, and 6 edges. (**b**) Cube, with four-, three-, and twofold symmetry, has 6 square faces, 8 vertices, and 12 edges. (**c**) Octahedron which has two- and threefold symmetry has 8 triangular faces, 8 vertices, and 12 edges. (**d**) Icosahedron with five-, three-, and twofold symmetry axes has 20 triangular faces, 12 vertices, and 30 edges. (**e**) Dodecahedron, which also displays the same 5-3-2 symmetry elements as an icosahedron, has 12 faces, 20 vertices, and 30 edges. In contrast to an icosahedron in which three triangular faces meet at a vertex, in the dodecahedron, three pentagonal faces meet at each of the vertices

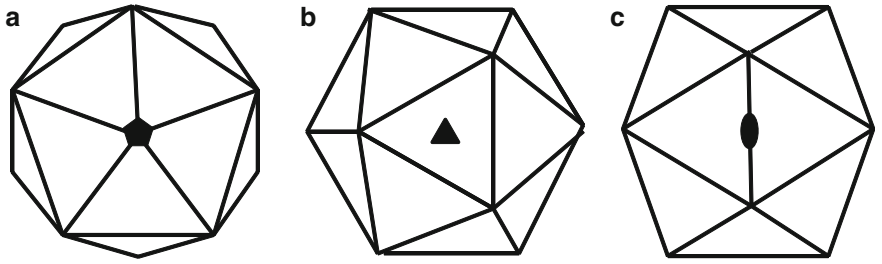


Fig. 3.2 Icosahedral axes of symmetry. An icosahedron displayed along the (**a**) five-, (**b**) three-, and (**c**) twofold symmetry axes. The fivefold rotation axis passes through the vertices of the icosahedron; the threefold axis passes through the middle of each triangular face; and the twofold axis through the center of each edge

opposite faces and six twofold symmetry axes going through the midpoints of opposite edges. Similarly, in an icosahedron, there are 12 vertices with fivefold rotational symmetry, 20 triangular faces with threefold symmetry, and 30 edges with twofold symmetry (Fig. 3.2). Among the platonic solids, fivefold rotational symmetry is present only in the icosahedron and its dual, the dodecahedron (Fig. 3.1). By analyzing the X-ray diffraction patterns obtained from the crystals of a spherical plant

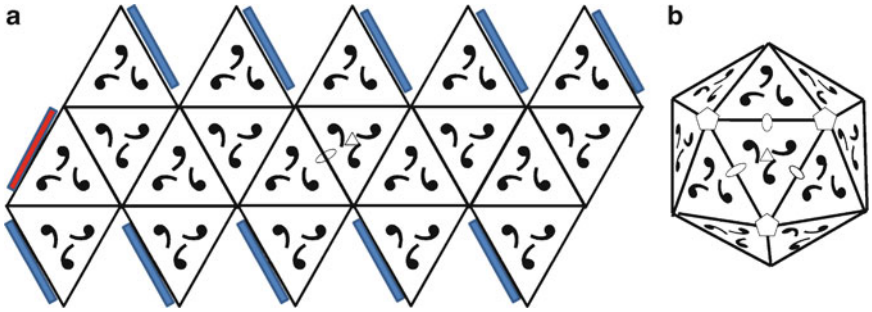


Fig. 3.3 Construction of an icosahedron from a template based on a planar hexagonal net. (**a**) The template consists of 20 equilateral triangles cut from a hexagonal net. Each triangle has a threefold axis at the center, indicated by a small triangle symbol, and a twofold axis at the center of the line that joins the adjacent triangles, indicated by an *oval* symbol. Application of the threefold rotational symmetry to a motif (*quotes*) placed in one of the triangles generates two other motifs in the same triangle, and successive application of the twofold rotational symmetry between the adjacent triangles results in each of the 20 triangles having three motifs as shown. To construct an icosahedron from this planar net, first, the two ends of the central body consisting of ten equilateral triangles are folded and glued at the edge shown as a *red band*. Each of the five triangular faces at the top is then joined with one another at the *blue bands* to form a single vertex, and a similar operation with the five triangular faces at the bottom results in an icosahedron with 12 fivefold vertices. (**b**) Hexagonal net in (**a**) folded into an icosahedron. The 60 motifs (*quotes*) in the icosahedron are now related by five-, three-, and twofold symmetry, indicated by a *pentagon*, *triangle*, and *oval* symbols, respectively

virus, tomato bushy stunt virus (TBSV), which showed characteristics spikes that only arise because of fivefold symmetry, Caspar provided the first evidence for the presence of icosahedral (5-3-2) symmetry in spherical viruses (Caspar 1956). Soon after, Klug, by analyzing the X-ray diffraction patterns from another spherical plant virus called tomato yellow mosaic virus (TYMV), provided further evidence for icosahedral symmetry in spherical viruses (Klug et al. 1957). At that time in the 1950s when these fundamental discoveries were made, the X-ray diffraction methods and the computer software were not adequately developed for determining the three-dimensional structures. However, later structural studies overcoming these technical limitations clearly established icosahedral capsid organization in a variety of spherical viruses.

3.3.2 Icosahedral Capsid Organization

The icosahedron with five-, three-, and twofold rotational symmetry axes allows placement of 60 identical units with equivalent contacts between each of them. In contrast, a cube with four-, three-, and twofold symmetry axes, as mentioned above, allows placement of 12 identical units. Placement of 60 units in an icosahedron can be illustrated by considering the construction of an icosahedron based on a hexagonal net (Fig. 3.3a). By placing a subunit at one corner of one of the 20 triangular facets, as a result of the threefold symmetry axis, passing through the center of the triangle and perpendicular to the plane of the triangle, the other two corners of this facet will have subunits, and then, as a result of repeated application of the twofold axis of symmetry, at the center of the edge joining the adjacent triangular facets, we generate 60 subunits that are related by 5-3-2 symmetry, with every subunit having an identical environment (Fig. 3.3b). A pertinent question at this point is whether all the spherical viruses with icosahedral symmetric capsids have only 60 identical subunits? Although there are a number of viruses in which capsid consists of 60 identical subunits, such as satellite plant viruses (Ban et al. 1995), there are many spherical viruses which consist of more than 60 subunits,

as was first shown by Brenner and Horne using EM of negatively stained virus specimens (Brenner and Horne 1959). From later studies, we know that not only do these viruses have more than 60 identical subunits but also, in several cases, the capsid is formed by subunits of different gene products. For simplicity, we will consider first how spherical viruses with more than 60 identical subunits, i.e., single gene product, conform to icosahedrally symmetric organization. Caper and Klug (1962) provided an elegant conceptual framework that specifically addressed this question.

3.3.3 Triangulation Numbers

It is clear from symmetry considerations that more than 60 identical subunits cannot be placed in such a way that they have strictly equivalent positions on an icosahedral surface. However, Casper and Klug (1962) argued that this can be achieved by allowing minimal distortions from the strict equivalence. To achieve this, with an assumption that size of the subunit remains the same and only the number of subunits varies, the basic triangular facet of the icosahedron has to be first enlarged and then subdivided into smaller triangles. Such a subdivision, which is referred to as triangulation for convenience in this discussion, cannot be arbitrary, and because of geometrical considerations, it is dictated by the equation $T = H^2 + HK + K^2$, where T is the triangulation number, and h and k are 0 or positive integers (Fig. 3.4). That is, the T number takes discrete values such as 1, 3, 4, 7, etc., and subdividing an equilateral triangle into, say, five or eight smaller triangles is not allowed.

The concept of triangulation and how it allows for more than 60 subunits with consequent increase in the size of the icosahedron can be illustrated using a hexagonal lattice with H- and K-axes crossing at 60° angle (Fig. 3.4a). By arbitrarily choosing a lattice point as the origin (0, 0) and considering it as the position of a fivefold vertex of an icosahedron, the position (H, K) of the neighboring fivefold vertex that is closest to the origin signifies the T number of that icosahedron. The equilateral triangle with the length of each side equal to the distance between the origin and the position (H, K) corresponds to one of the 20 triangular faces of such an icosahedron with each of its corners representing a fivefold vertex. The icosahedron with no triangulation can be described as having a triangulation number of 1 ($T = 1$) in which the closest fivefold vertex is positioned at ($H = 1$, $K = 0$). By defining the equilateral triangle representing each face in such a $T = 1$ icosahedron as a unit triangle, in a $T = 4$ icosahedron, for example, with closest fivefold vertex positioned at ($H = 2$, $K = 0$), the equilateral triangle describing each facet consists of four unit triangles (Fig. 3.4a). That means, in each triangular facet of the $T = 4$ icosahedron, 12 subunits can be placed, in contrast to three subunits in the facet of the $T = 1$ icosahedron. With 12 subunits in each of the 20 facets, a $T = 4$ icosahedron then will accommodate 240 (60T) subunits in contrast to 60 subunits in the $T = 1$ icosahedron (Fig. 3.4b). Also, as can be seen, the size of the $T = 4$ icosahedron compared to the size of the $T = 1$ icosahedron has proportionally increased. It should be pointed out here that subdividing the triangular facet resulting in icosahedra with $T > 1$ need not necessarily increase the size and that increased size is only with the assumption that molecular mass of the subunit remains approximately the same. Generally, however, spherical viruses with $T > 1$ tend to be of larger size.

3.3.4 Classes of Icosahedra

Based on their T numbers, icosahedra can be divided into three classes (Fig. 3.5). In the first class, icosahedra have T numbers based on the H-axis (1, 4, 9, etc.) with $H \geq 1$ and $K = 0$. In these icosahedra, lattice lines run parallel to the edges of the triangular icosahedral facet. In the second class, the icosahedra have T numbers along the line that bisects H- and K-axes (3, 12, 27, etc.) with $H = K$. In this class of icosahedra, the lattice lines bisect the angles between the edges of the icosahedral

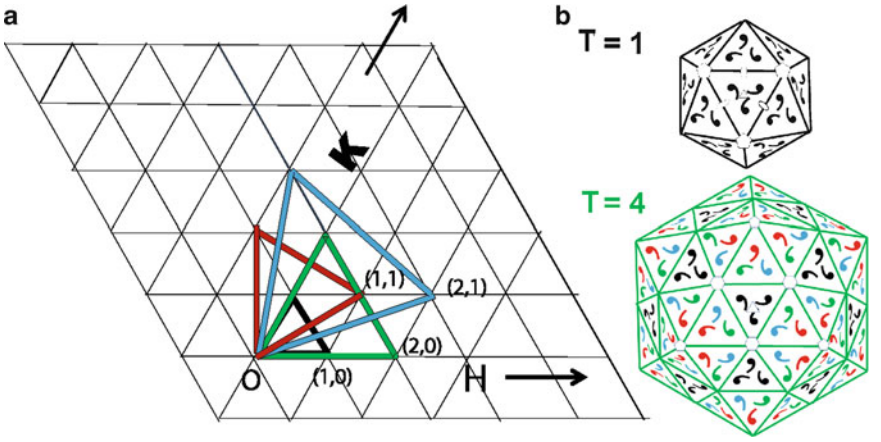


Fig. 3.4 Triangulated icosahedral lattices. (**a**) The hexagonal net used for constructing an icosahedron in Fig. 3.3 also serves to illustrate the formation of equilateral facets in the triangulated icosahedral lattices. The facet of the triangulated lattice of an icosahedron of a given T number is specified by a vector **T** (H, K) from the origin (**O**). The unit vector **T** (1, 0) (*black*) in this representation specifies the facet of the basic $T=1$ icosahedron. Other vectors such as **T** (1, 1), **T** (2, 0), and **T** (1, 2), for example, form the basis for successively larger $T=3$ (*red*), $T=4$ (*green*), and $T=7$ (*blue*) icosahedral facets, respectively. To construct a triangulated icosahedral lattice of a particular T number ($=H^2+HK+K^2$), its facet, which is an equilateral triangle, is generated, as specified by the vector **T** (H, K), using the underlying planar hexagonal net. Nineteen other triangles are then generated to give a template, as in Fig. 3.3, for constructing an icosahedron with a given T number. The *black*, *red*, *green*, and *blue triangles* represent facets for the $T=1$, 3, 4, and 7 icosahedra, respectively. Each vertex of the facet triangle becomes fivefold when the template is folded into an icosahedron as shown in Fig. 3.3. (**b**) The folded $T=1$ ($H=1$, $K=0$) and $T=4$ ($H=2$, $K=0$) templates, in *black* and *green*, respectively, are shown for comparison. The subunit organization in these icosahedra is shown using *quotes* to represent a "subunit" as in Fig. 3.3. In contrast to the $T=1$ icosahedron, which has 20 unit triangles, specified by the vector **T** (1, 0), with 60 subunits, the $T=4$ lattice, specified by **T** (2, 0), consists of 80 ($20T$) unit triangles with 240 ($60T$) subunits. The folded $T=4$ icosahedron clearly illustrates how the nonvertex sixfold positions in the net remain hexavalent (indicated by *hexagon* symbols) whereas the vertex sixfold positions in the net become pentavalent (indicated by *pentagon* symbol) upon folding. As in any triangulated icosahedron, with the exception of the unit triangle at the icosahedral threefold position, the other triangles exhibit local (or quasi) threefold symmetry; similarly, the adjacent unit triangles are related by local (or quasi) twofold axes, unless the midpoint of the edge coincides with icosahedral twofold axis. Each facet in the $T=4$ icosahedron is comprised of four triangles. The icosahedral threefold axis, at the center of the facet, divides the facet into three equivalent parts. Each part, consisting of one-third of the central triangle and one of the remaining three triangles in the facet, constitutes the icosahedral asymmetric unit. The four "subunits" in the asymmetric unit, one from the central triangle and three from one of the other triangles in facet, are shown in different colors to indicate their quasi-equivalent environment. The subunit in the central triangle is colored in *black*, while the subunits in the other triangle are colored in *red*, *blue*, and *green*. Application of the strict five-, three-, and twofold rotations to these quasi-equivalent subunits in the asymmetric unit generates rest of the 240 subunits. The arrangement of the subunits clearly illustrates how the triangulation leads to the formation of the rings of 5 (*red* subunits) and 6 (*black*, *green*, and *blue* around the hexavalent points) because of the triangulation. Furthermore, it also illustrates that although the formation of rings of 5 and 6 in a triangulated lattice is a geometrical necessity, clustering of the subunits into pentamers and hexamers is not obligatory. In the $T=4$ icosahedron shown here, either each subunit can be considered separately or as a cluster of three subunits (trimer). With a trimer as the building block, one trimer (*three black* subunits) occupies the central triangle of the facet, at the icosahedral threefold position, and another "quasi-equivalent" trimer (*red*, *green*, and *blue* subunits) occupies the other triangle in the facet. Such a $T=4$ organization with trimers is observed in the case of alphaviruses (see Fig. 3.12). See Figs. 3.7a and 3.8a for folded $T=3$ (*red* facet) and $T=7$ (*blue* facet) icosahedral lattices, respectively

facet. The third class, called the skew class, includes icosahedra with other allowed T numbers (7, 13, 19, 21, etc.), in which the lattice lines are not symmetrically disposed with respect to the edges of the icosahedral facet. In the first two classes, the lattice points that signify the T number are uniquely defined, whereas in the skewed class, there are two possibilities for the lattice points that define their T numbers. For example, for $T=7$ ($H=2$, $K=1$) and ($H=1$, $K=2$) are equally possible.

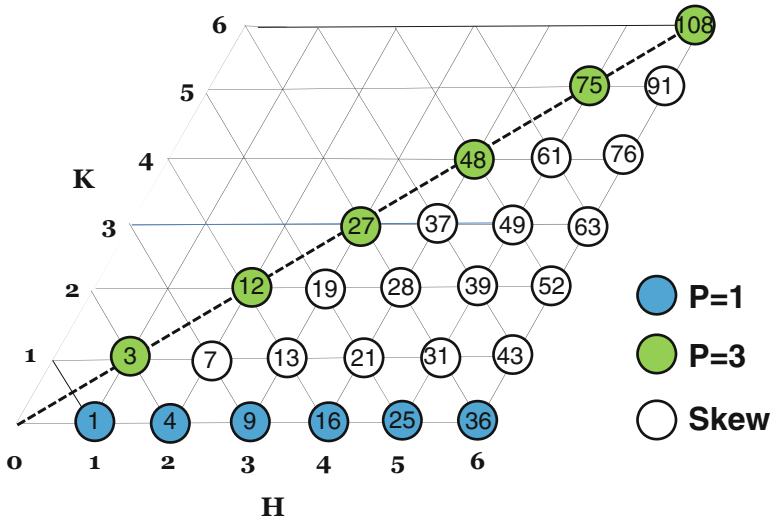


Fig. 3.5 Different classes of icosahedra. The origin ($H=0$, $K=0$) in the equilateral triangular net represents the position of a fivefold vertex of an icosahedron, and the position of the neighboring fivefold vertex in that icosahedron is represented at a position (H, K) based on its T number (shown inside the *circles*). The icosahedra with $K=0$ (or $H=0$) belong to $P=1$ class (*blue-filled circles*). The icosahedra with $H=K$ (on the *dashed line*) belong to $P=3$ class (*green-filled circles*). All other icosahedra belong to the skew class (*open circles*). These icosahedra exhibit lattices with handedness. Skewed icosahedra with $H>K$, below the *dashed* $H=K$ *line*, are left-handed (*laevo*) lattices, and those with $H<K$, above the *dashed line*, are right-handed lattices (*dextro*)

These two represent left-handed (*leavo*) and right-handed (*dextro*) enantiomorphic configurations. Examples of virus structures with skew icosahedral lattice include polyomaviruses ($T=7d$), bacteriophage ($T=7d$), and rotavirus ($T=13l$). In the literature, the first and second classes of icosahedra are also referred to as $P=1$ and $P=3$ classes, respectively, by defining the T number as $T=Pf^2$. In this equation, f is the largest common divisor between H and K, and $P=h^2+hk+k^2$, where h and k are integers without any common factor. All icosahedra with $P\geq 7$ belong to skew class.

Another form of icosahedron that is found in some viruses such as phi29 (Tao et al. 1998), T-even bacteriophages (Fokine et al. 2004; Rao and Black 2010), and aberrant flock house virus particles (Dong et al. 1998; Wikoff and Johnson 1999) is the prolate icosahedron. Here, the icosahedron is stretched along one of the icosahedral axes. A typical icosahedron can be considered as having a central cylindrical body, consisting of ten triangles, with two caps, each with five triangles, at its bottom and the top (Fig. 3.6a). The prolate icosahedra are characterized by a combination of T number and an elongation number called Q according to the formula $n=30(T+Q)$ (Fig. 3.6b), where T is the triangulation number as defined previously, Q is any positive integer, that defines the triangulation number for the central body, and n refers to number of subunits (Fokine et al. 2004). In the triangles that constitute the caps, the triangulation follows the T number, whereas in the triangles that constitute the main cylindrical body, it follows the Q number. As can be seen, when $T=Q$, then the icosahedra become isometric with $n=60T$, as discussed above. When $Q>T$, the resulting icosahedron is referred to as a prolate icosahedron, and when $Q<T$, it is referred to as an oblate icosahedron. The structure of T4 bacteriophage exhibits a prolate icosahedron with $T=13$ and $Q=21$ (Fokine et al. 2004) (Fig. 3.6c), whereas the major capsid of the phi29 exhibits a prolate icosahedron with $T=3$ and $Q=5$ (Tao et al. 1998).

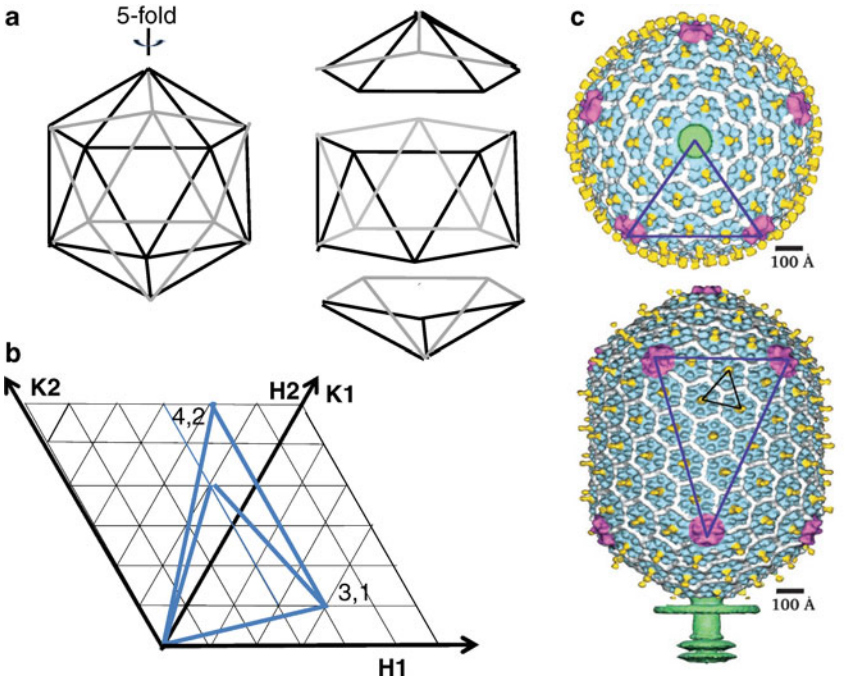


Fig. 3.6 Prolate icosahedra. (**a**) Illustration of how an icosahedron (*left*) can be considered as having two end caps, each with five triangular faces separated by a central cylindrical body consisting of ten triangular faces right. (**b**) Representation of T and Q numbers on an equilateral triangular net in a prolate icosahedron. The prolate icosahedra have two types of facets, one in the end caps and the other in the central body with unequal sides. The triangulation in these two facets can be represented on a hexagonal net by considering two coordinate points ($H1$, $K1$) and ($H2$, $K2$) (Moody 1999; Fokine et al. 2004). The vector from the origin to the point ($H1$, $K1$) specifies the equilateral facet for the end caps as in Fig. 3.4, whereas the facet for the central body with unequal sides is specified by two vectors, one from the origin to the point ($H1$, $K1$) and the other from the origin to the point ($H2$, $K2$). The triangulation in the equilateral facets of the end caps is defined as $T\ (H1,\ K1) = H1^2 + H1K1 + K1^2$ as illustrated in Fig. 3.4, whereas the triangulation in the facet, with unequal sides, of the central body is defined by $Q = H1H2 + H1K2 + K1K2$. As an example, the triangulation in the prolate icosahedron with $T = 13l$ ($H1 = 3$, $K1 = 1$) in the end caps and $Q = 20$ ($H2 = 4$, $K2 = 2$) in the central body is illustrated here. (**c**) Surface representation of the cryo-EM reconstruction (adapted from Fokine et al. 2004, with permission from Dr. M.G. Rossmann) of the T4 bacteriophage head illustrating subunit arrangement in the $T = 13$ lattice in the end caps (*above*), shown along the fivefold axis, and in the $Q = 20$ lattice in the central body (*below*). The facets in both the lattices are indicated

3.3.5 Icosahedral Asymmetric Unit and Quasi-Equivalent Subunits

An important concept that emerges from the triangulation is the icosahedral asymmetric unit. The threefold rotational symmetry axis passing through the center of the triangular icosahedral facet divides the subunits in the facet into three symmetrically equivalent sets. Each set of the subunits is defined as one icosahedral asymmetric unit, and application of the 5-3-2 rotational symmetry to this asymmetric unit produces all the $60T$ subunits in the icosahedron. In a $T = 1$ icosahedron, the asymmetric unit consists of one subunit, whereas in a $T = 4$ icosahedron, for example, the asymmetric unit consists of four subunits (Fig. 3.4b). As the interacting environment between these subunits in the icosahedron with $T > 1$ cannot be strictly equivalent, they are termed as "quasi-equivalent" subunits (black, blue, red, and green commas in Fig. 3.4b). Caspar and Klug proposed that these quasi-equivalent subunits in the icosahedral shell retain similar bonding interactions with minor distortions in their intersubunit interactions in order to adapt to the nonsymmetry-related environments.

3.3.6 *Pentavalent and Hexavalent Positions*

Another important consequence of the "quasi-equivalence" theory developed by Caspar and Klug is that triangulation necessarily results in the generation of hexavalent (sixfold) locations in addition to pentavalent (fivefold) positions on the icosahedral lattice (Fig. 3.4b). Irrespective of the T number, all icosahedra necessarily have 12 pentavalent positions. In the icosahedra with $T>1$, because of the triangulation, $10(T-1)$ hexavalent positions are generated. As a result, in icosahedra with $T>1$, the $60T$ subunits could cluster into 12 pentamers around the fivefold vertices and $10(T-1)$ hexamers at the hexavalent lattice points. Caspar and Klug defined these subunit clusters as morphological units. An icosahedron with a specific T number will then have $10(T+2)$ morphological units [i.e., $10(T-1)$ hexamers + 12 pentamers]. Although the arrangement of $60T$ subunits into rings of 5 and 6 is a geometrical necessity, clustering of these subunits into pentamers and hexamers is not; clustering into $20T$ trimers, $30T$ dimers, or $60T$ monomers is possible (Fig. 3.4b). Casper and Klug argued that if a particular oligomeric state, for example, hexamers, if they are particularly stable, they might be preformed, but when they are assembled into the shell, these conceptually planar units would have to be transformed into convex pentamers, resulting from the removal of a subunit, to occupy the "domed" pentavalent positions in the icosahedral structure. They suggested that such transformation would only require minor alterations in the dihedral angles between the subunits but essentially maintaining similar intersubunit contacts.

3.4 High-Resolution Structures of Spherical Viruses and Quasi-Equivalence Theory

Two basic tenets of the quasi-equivalence theory as discussed above are that (1) the icosahedral lattice with the possibility of triangulation presents the most efficient geometrical design for close packing of identical subunits in a spherical shell and (2) that the structural organization involves quasi-equivalent interactions requiring minimal distortions in the subunit bonding. Since the proposal of this theory in 1962, in the last three decades, high-resolution structures of several spherical viruses of different sizes have been determined. These structures clearly established that the capsid organization in spherical viruses follows icosahedral symmetry and that in viruses with subunits greater than 60, capsid organization is based on a triangulated icosahedral lattice as suggested from the quasi-equivalence theory. For example, several ssRNA plant viruses and some human viruses such as noroviruses, with capsid composed of 180 copies of the capsid protein, exhibit the expected $T=3$ icosahedral organization with rings of five and six subunits. In dsDNA bacterial viruses, such as P22 (Jiang et al. 2003), HK97 (Wikoff et al. 2000), with 420 copies of the capsid protein, the capsid organization is based on the expected $T=7$ icosahedral lattice with 60 hexamers and 12 pentamers. However, there are major surprises as well. The capsid organization in papovaviruses (papilloma- and polyomaviruses) represents a stunning departure from the quasi-equivalence theory (Liddington et al. 1991; Wolf et al. 2010). In these dsDNA spherical viruses, the capsid consists of 360 copies of the major capsid protein VP1. Such a number cannot be accommodated on a triangulated icosahedral lattice because $T=6$ (360/60) is forbidden as it does not adhere H^2+HK+K^2 rule (see above). Initially, although in conflict with the biochemical analysis which indicated 360 copies of the capsid protein in these virus, based on EM images of negatively stained specimens and computer reconstruction, an icosahedral structure with 420 copies organized as 60 hexamers and 12 pentamers on a $T=7$ icosahedral lattice, as expected from the quasi-equivalence theory, was proposed (Klug and Finch 1968). However, subsequent high-resolution structures of these viruses unambiguously revealed that the capsid indeed consists of 360 subunits and that these subunits, instead of pentamer–hexamer clustering,

are organized as 72 pentamers at 60 hexavalent and 12 pentavalent location on a triangulated $T=7d$ icosahedral lattice. (Liddington et al. 1991; Wolf et al. 2010) Other examples include adenovirus, a dsDNA virus, in which 240 trimers of the major capsid protein (hexons) occupy hexavalent positions on a $T=25$ (pseudo) icosahedral lattice (Roberts et al. 1986; Liu et al. 2010; Reddy et al. 2010) and a unique icosahedral organization with 120 (forbidden $T=2$) subunits which is a recurring theme in dsRNA viruses including fungal L-A virus (Naitow et al. 2002), partitivirus (Ochoa et al. 2008), and inner shells of bluetongue virus (Grimes et al. 1998), rotavirus (Lawton et al. 1997; Chen et al. 2006; Settembre et al. 2011), and reovirus (Reinisch et al. 2000).

3.4.1 Conformational Switching

Although the high-resolution structures of spherical viruses show general concordance with the quasi-equivalent theory in terms of subunit arrangement on triangulated icosahedral lattices, they exposed limitations of the theory particularly in regard to the concept of quasi-equivalent interactions that bond the subunits in the context of icosahedral lattice. These structures showed that formation of the icosahedral capsid can be governed by nonequivalent interactions involving internally located conformationally "flexible" arms of the capsid protein subunits. Except for these conformationally flexible arms, which function as molecular switches to allow the subunits to adapt to quasi-equivalent environments of the triangulated icosahedral lattice, the majority of the capsid protein remains structurally invariant.

Capsid organization in many small plant and animal viruses follows $T=3$ icosahedral symmetry with 180 chemically identical subunits (Fig. 3.7). In a $T=3$ lattice (Fig. 3.7a), the icosahedral asymmetric unit consists of three quasi-equivalent subunits conventionally referred to as A, B, and C (Rossmann and Johnson 1989). These subunits form two types of quasi-equivalent dimers: A/B dimers, located at quasi-twofold axis of the $T=3$ lattice, and C/C dimers, located at the icosahedral twofold axis (Fig. 3.7b). Thus, the capsid consists of 60 A/B dimers and 30 C/C dimers. The A/B dimers surround the fivefold vertex forming rings of 5, and at the six-coordinated positions, A/B and C/C dimers alternate to form rings of 6. Despite lacking any sequence homology, the domain that participates in the formation of the icosahedral shell in these viruses exhibits a highly conserved polypeptide fold. This fold with two flanking twisted β-sheets, each consisting of four antiparallel β-strands, is called the eight-stranded jelly roll β-barrel motif (Fig. 3.7c). How do the dimers conform to the quasi-equivalent environment of the $T=3$ lattice and form a closed spherical shell? In conforming to the curvature of the spherical shell, A/B dimer exhibits a bent conformation whereas the C/C dimer is flat (Fig. 3.7d). Despite some thematic variations between the viruses, the internally located flexible N-terminal arm (NTA) is implicated in providing a switch to facilitate bent A/B and flat C/C conformations during $T=3$ capsid assembly (Fig. 3.7e). In the plant tombus viruses (Harrison et al. 1978; Hogle et al. 1986) and sobamoviruses (Abad-Zapatero et al. 1980), the NTA of the C subunit is ordered, whereas the equivalent regions in the A and B subunits are disordered, providing a switch to allow bent and flat conformations of the A/B and C/C dimers, respectively. In nodaviruses, an ordered arm of the C subunit and a piece of genomic RNA are implicated in keeping the flat conformation of the C/C dimers (Fisher and Johnson 1993). In human noroviruses, the ordered NTA of the B subunit, which interacts with the base of the shell domain of the neighboring C subunit, is suggested to provide such a switch (Prasad et al. 1999). Thus, in these viruses, at the level of the NTA, the $T=3$ icosahedral symmetry is reduced to $T=1$ with only one of the three NTAs of the quasi-equivalent subunits being ordered. The structures of animal caliciviruses exhibit a novel and distinct variation from any of these viruses (Chen et al. 2006; Ossiboff et al. 2010). The NTAs of A, B, and C in these viruses are equally ordered and provide a network of interactions essentially maintaining the $T=3$ symmetry at this level. Instead of an order-to-disorder transition as described

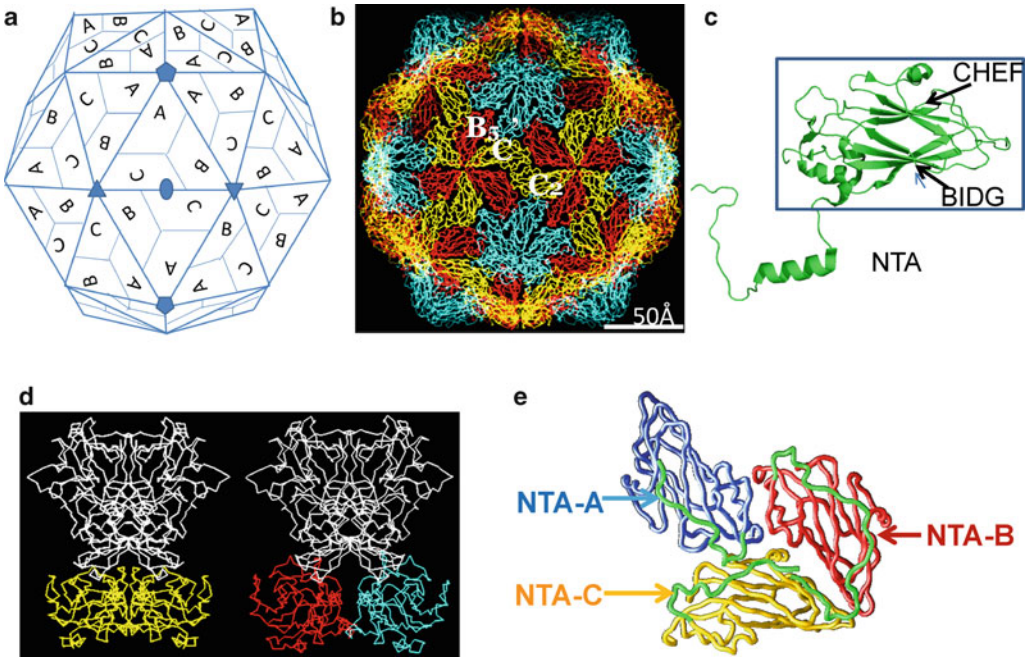


Fig. 3.7 Subunit organization and conformational switching in $T=3$ icosahedral viruses. (**a**) $T=3$ lattice as viewed along the icosahedral twofold axis. A set of five-, three-, and twofold axes of the $T=3$ icosahedron are denoted. The three quasi-equivalent "subunits" in the asymmetric unit of the $T=3$ lattice are indicated by A, B, and C. In a $T=3$ structure, these subunits are chemically equivalent. Application of the icosahedral symmetry generates 60 sets of these quasi-equivalent subunits. Disposition of the symmetry-related subunits is also indicated. The formation of the rings of 5 and 6 is clearly seen. The A subunits cluster around the fivefold axis, whereas B and C alternate around the six-coordinated positions. (**b**) The packing of the canonical trapezoid-shaped β-barrel domains as typically observed in a $T=3$ icosahedral virus structures. The view is along the icosahedral twofold axis, same as in (**a**). The β-barrels corresponding to the quasi-equivalent A, B, and C in (**a**) are colored in *cyan*, *red*, and *yellow*, respectively. The icosahedral shell can be considered as built from 60 A/B to 30 C/C dimers. The A/B dimers are related by local twofold symmetry (AB_5 in the figure), and C/C dimers are related by icosahedral symmetry (C/C_2 in the figure). (**c**) A typical jelly roll β-barrel domain [taken from the structure of San Miguel sea lion virus (Chen et al. 2006), an animal calicivirus] that participates in the $T=3$ icosahedral shell. The β-barrel motif (inside the *box*) consists of eight β-strands organized into two twisted antiparallel β-sheets generally referred to as BIDG and CHEF (Rossmann and Johnson 1989). The letters refer to the position of β-strands in the primary sequence: B is the most N-terminal, and H is the most C-terminal. An N-terminal arm that projects inward from the β-barrel participates in the intersubunit interactions. (**d**) Comparison of the C/C2 (*left*) and A/B5 (*right*) dimers in the Norwalk virus $T=3$ structure (Prasad et al. 1999) showing the flat and bent conformations, respectively. In Norwalk virus, the capsid protein consists of two domains: the shell domain (S), with a β-barrel motif, and a protruding domain (P). Only the S domain participates in the shell contacts. The β-barrel domains of A, B, and C are colored as in (**b**). The P domain which participates in the dimeric interactions is colored in *white*. Although structurally not similar, capsid protein of tombus viruses, such as TBSV, also has a protruding (P) domain (Harrison et al. 1978). (**e**) Nonequivalent interactions, as viewed from inside of the capsid, between the NTAs of the ABC subunits that are observed in the Norwalk virus structure, shown here for example (see text). The NTAs (*green*) from different subunits are marked. The ABC subunits are shown using the same color scheme as in (**b**)

above, a distinct conformational change involving a Pro residue in the B subunit that leads to the formation of a ring-like structure around the fivefold axis appears to provide a switch. In several of these viruses, the role of NTA in conferring correct capsid assembly is substantiated by mutational studies. Deletion of NTA in the sobamovirus results in formation of a $T=1$ structure (Erickson et al. 1985), mutation of NTA residues involved in the RNA interactions in nodaviruses results in aberrant particles (Dong et al. 1998; Wikoff and Johnson 1999), and deletion of N-terminal 35 residues in norovirus results in abrogation of capsid assembly (Bertolotti-Ciarlet et al. 2002).

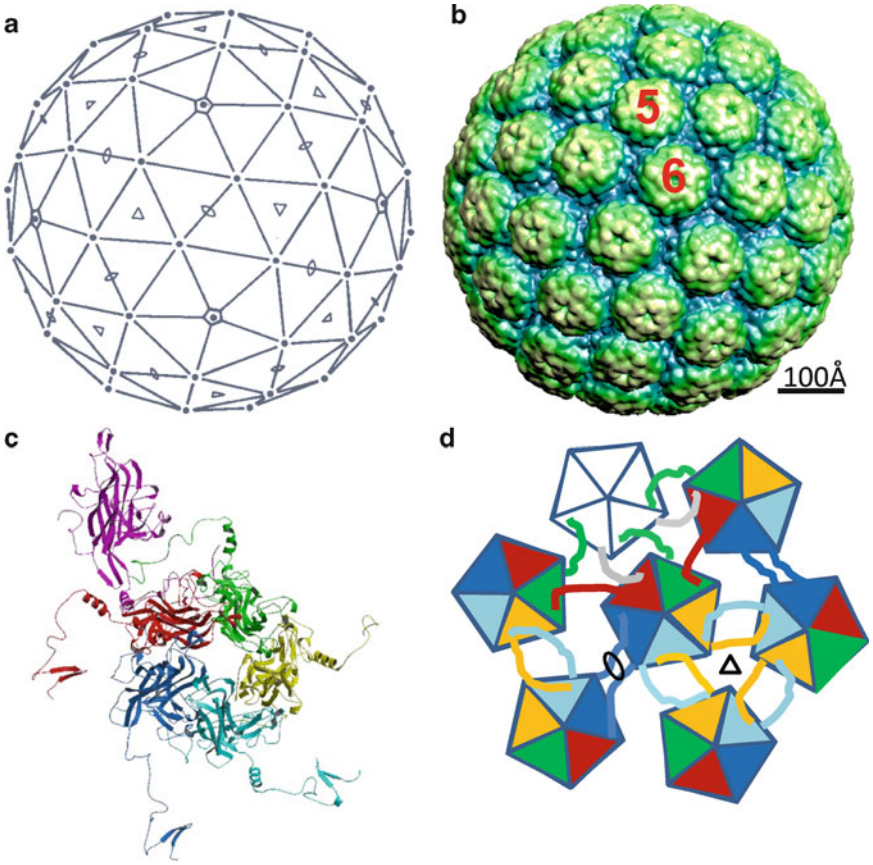


Fig. 3.8 Subunit packing and intersubunit interactions in the all-pentamer $T=7$ structure of polyomavirus. (**a**) $T=7$ icosahedral lattice as viewed along the icosahedral twofold axis. The five-, three-, and twofold symmetry elements are denoted by *pentagon*, *triangle*, and *oval* symbols. (**b**) Crystallographic structure of polyomavirus, viewed along the twofold axis as in (**a**), showing the close packing of pentamers on a $T=7$ icosahedral lattice (obtained from VIPER, Reddy et al. 2001). Pentamers sit on the five- and six-coordinated positions of the lattice. Two of these locations are denoted. (**c**) The icosahedral asymmetric unit consisting of a pentamer at the six-coordinated position and a subunit (shown in *pink*) from the pentamer at the fivefold axis. The subunits in the pentamer were colored differently (obtained from VIPER, Reddy et al. 2001). Application of the five-, three-, and twofold symmetry generates the structures shown in (**b**). The CTAs emerging from each subunit are clearly seen. (**d**) A schematic representation of the interchange of CTA arms between the pentamers that hold the capsid together (Liddington et al. 1991). The pentameric subunits are depicted as *triangles* inside a *pentagon*. The subunits in the pentamers at the sixfold node are colored in different colors as in (**c**). The pentamer at the fivefold axis is shown in *white*. The CTAs emerging from each subunit is shown in the same color as the subunit. The CTA from the pentavalent pentamer is shown in *gray*. Three distinct types of inter-pentameric interactions involving interchange of CTAs are observed in the structure. First type, between the pentavalent pentamer and two hexavalent pentamers related by the local threefold axis (*gray*, *red*, and *green* CTAs), between the two hexavalent pentamers related by the local twofold axis (*yellow* and *cyan*), and the third type, between the hexavalent pentamers related by the icosahedral twofold axis (*blue–blue*)

Conformational switching, as observed in the case of $T=3$ icosahedral viruses, is also evident in the capsid structure of in papovaviruses with all-pentamer arrangement on a $T=7$ icosahedral lattice (Liddington et al. 1991; Wolf et al. 2010), as mentioned earlier (Fig. 3.8a, b). In this structure, there are two types of pentamers, one located at the pentavalent lattice points of the $T=7$ lattice and the other located at the hexavalent lattice points (Fig. 3.8b). Each pentamer exhibits a roughly cylindrical shape with a hollow conical interior (Fig. 3.8c). Except for the flexible C-terminal arm (CTA),

the subunits that compose both types of pentamers exhibit a similar structure. Interestingly, the main body exhibits the same canonical eight-stranded jelly roll β-barrel fold as the subunits in the $T=3$ icosahedral viruses except that the long axis of this fold is oriented radially in the polyomavirus in contrast to a tangential orientation in the $T=3$ viruses. The subunits in the pentavalent pentamer surrounded by five hexavalent pentamers have identical environments. However, the local environment for the subunits in the hexavalent pentamer, surrounded by a pentavalent pentamer and five other hexavalent pentamers, varies. How do these subunits conform to these local variations? The situation is analogous to the two quasi-equivalent dimers in the $T=3$ structures. Instead of a flexible NTA as in $T=3$ viruses, in papovaviruses, the flexible CTA of the capsid protein subunit provides the molecular switch to adapt to the local environment. The CTA extending away from the main body of each pentameric subunit invades the subunit of an adjacent pentamer such that each pentamer receives and donates five arms (Fig. 3.8d). The required variability for the capsid formation comes from the manner in which the conformationally flexible CTA are exchanged between the adjacent pentamers in the $T=7$ icosahedral lattice.

3.4.2 Triangulated Lattice and Subunit Packing

One of the main tenets of the quasi-equivalence theory that triangulated icosahedral lattices allow for efficient close packing of subunits is clearly evident in the high-resolution structures of spherical viruses including the papovaviruses. However, there are distinct variations in how triangulated lattices confer optimal subunit packing. The all-pentamer papovavirus structure represents a unique variation in which subunit packing involves a triangulated lattice despite the mismatch between the molecular symmetry and the lattice coordination. Except for the 12 pentamers at the fivefold positions of the $T=7$ lattice, the location of other pentamers, at the six-coordinated positions, is not consistent with their molecular symmetry. The advantage, however, is clearly evident considering that a triangulated lattice intrinsically provides locations for efficient hexagonal close packing of the subunits. The papovavirus structures elegantly demonstrate how the six-coordinated positions in the $T=7$ lattice allow for a favorable close packing of the roughly cylindrical pentamers between the fivefold positions requiring only three different types of interpentamer contacts (Fig. 3.8d).

In the $T=3$ structures with 180 identical subunits, as discussed previously, the subunit packing is as per the quasi-equivalent theory. The trapezoidal-shaped β-barrel domains of the capsid protein pack closely into rings of 6 at the hexavalent lattice points and rings of 5 around the pentavalent positions. Structures of picornaviruses (Hogle et al. 1985; Rossmann et al. 1985; Luo et al. 1987; Acharya et al. 1989) present an interesting variation depicting how a $T=3$ lattice allows similar packing but with nonidentical subunits. In picornaviruses, the icosahedral asymmetric unit consists of chemically nonidentical VP1, VP2, and VP3. Despite not having any sequence homology with capsid proteins of $T=3$ viruses or with themselves, VP1, VP2, and VP3 exhibit the same canonical β-barrel fold. The arrangement of 180 β-barrels, from 60 copies of each of the VP1, VP2, and VP3, is strikingly similar to that observed in the $T=3$ icosahedral lattices formed by 180 identical copies of a capsid protein. In the picornavirus structures, VP1, VP3, and VP2 occupy the same positions as chemically equivalent A, B, and C, respectively, in the $T=3$ icosahedral viruses. Because VP1, VP2, and VP3 are chemically nonidentical, the picornavirus structures are described as a pseudo $T=3$ lattice. The pseudo $T=3$ organization in the comovirus provides yet another interesting variation with two chemically distinct polypeptide chains, the small (S) protein with one β-barrel domain and the large (L) protein with two β-barrel domains (Lin et al. 1999). The packing of the β-barrels from these two proteins follows $T=3$ lattice and is similar to that observed in the $T=3$ icosahedral structures. The β-barrel of the S protein occupies the position corresponding to A in the $T=3$ lattice, whereas the two β-barrels of the L protein occupy positions corresponding to B and C.

3.4.3 Capsid Assembly

In an attempt to answer what dictates appropriate conformational switching in the formation of icosahedral shells, Berger et al. (1994) has proposed a local rule-based theory suggesting that protein subunits make use of local information to guide the capsid assembly and that the choice for a particular interaction is dictated by its immediate neighbors. In the $T=3$ icosahedral viruses, dimer of the capsid protein is thought to be the building block for the assembly. In solution, these dimers are perhaps in a dynamic equilibrium between the "bent" and "flat" conformations, and during the assembly, these dimers adopt appropriate conformational states. Two different assembly pathways have been proposed for the $T=3$ icosahedral viruses. In the case of sobamoviruses, such as southern bean mosaic virus (SBMV), it is suggested that assembly involves the formation of pentamers of dimers as an intermediate step followed by the association of other dimers resulting in the formation of a $T=3$ shell (Erickson et al. 1985). Such a pathway is consistent with the observation that deletion of NTA in the SBMV results in a $T=1$ structure formed by the association of 12 pentamers of dimers. A similar pathway involving pentamers of dimers as an assembly intermediate is also proposed for noroviruses (Prasad et al. 1999), which is supported by recent mass spectroscopic analysis of recombinant Norwalk virus particles (Shoemaker et al. 2010). In the case of tombus viruses, such as TBSV, it is suggested that the assembly intermediate involves trimers of dimers, consistent with the observation that the ordered NTAs of the C subunits form a stable internal structure at the icosahedral threefold axes of the $T=3$ shell (Sorger et al. 1986). These viruses have a stretch of basic residues at the N terminus (R arm) of the capsid protein that can interact with the RNA. The intermediate assembly unit, either pentamers of dimers or trimers of dimers, is thought to be nucleated by interaction with the packaging signal in the genomic RNA (Sorger et al. 1986; Harrison 2007). In the case of noroviruses, the capsid protein, lacking the basic R arm, itself has all the determinants for the formation of the $T=3$ structure because the recombinant capsid protein of noroviruses readily assembles into $T=3$ structures (Prasad et al. 1999). The role of RNA in directing the assembly pathway is readily apparent in the structure for flock house virus (a nodavirus) (Fisher and Johnson 1993). For picornaviruses, the assembly pathway is somewhat better characterized. The 5S structural unit consisting of one copy of VP0, VP3, and VP1 and 14S pentameric caps of VP1–VP2–VP3 are known to be the intermediates. In the case of papovaviruses, in which preformed stable pentamers are the building blocks, the correct assembly of the pentamers onto a $T=7$ lattice is likely dictated by interactions with the viral minichromosome. Initial interactions between the pentamer and the DNA, involving the N-terminal arms of the subunits, may serve as a nucleation center for further stepwise addition of individual pentamers or a cluster of pentamers, consisting of one pentavalent pentamer surrounded by five other pentamers (1+5 cluster), to form the T=7 capsid structure with the encapsidated genome (Stehle et al. 1996; Mukherjee et al. 2007). During this process, the curvature is appropriately modulated by local alterations in the "bonding" between the pentamers involving the CTAs.

As can be seen from the above discussion, the interplay between the global restraints, which allow optimal packing of the subunits to form a closed shell of proper size to accommodate the genome, and local conformational variability, which allows, necessary flexibility in the intersubunit contacts for modulating the curvature, dictates structural realization in icosahedral viruses.

3.4.4 Scaffolds, Glue Proteins, and Cores

In more complex icosahedral viruses such as dsDNA bacteriophages, herpes simplex viruses, and adenovirus, the establishment of the icosahedral lattice involves several other factors like scaffolding proteins, accessory proteins, maturation-dependent proteolysis, and even larger-scale conformational changes in their major capsid proteins than is observed in simpler icosahedral viruses.

In contrast to assembly based on the encapsidation of the nucleic acid concurrently with the formation of the capsid shell by stepwise addition of smaller assembly intermediates as discussed in the previous section, in some of these viruses, capsid assembly is accomplished by the formation of a complete capsid shell, followed by the insertion of the nucleic acid. Such a mechanism avoids some of the problems associated with the former assembly mechanism, such as the requirement that both the capsid proteins and the nucleic acid be brought to a common assembly point and properly staged for assembly, and the necessity of using a nonicosahedral component (the RNA) to help build an icosahedral capsid. However, this mechanism introduces other problems that must be solved. First, since most dsDNA phages and viruses packaged by this mechanism have a single genome segment, it is absolutely required that only one copy of the nucleic acid be inserted into each capsid shell. This is accomplished by having a DNA packaging machine, called the portal, located at only one of the 12 vertices of the capsid (see also Chap. 22). Second, the capsid shell must be of the correct size to fit the nucleic acid genome, and it must be empty of cellular proteins, which could interfere with DNA insertion. This is accomplished by assembling the capsid around a set of virally encoded scaffolding proteins. Thus, the shell is guaranteed to be the right size and T number, and the scaffolding proteins are removed either during DNA insertion or by proteolysis after capsid shell assembly. Third, in the cases studied so far, the capsid proteins of the procapsid have a different conformation that they do in the mature virion. This could serve as a signal that the DNA has been packaged, and is ready for the final steps of virus maturation, like the addition of the phage tail. Finally, the DNA insertion is accompanied by an increase in internal pressure generated by the repulsion of the charged nucleic acid. This pressure may be as high as 40 atm and has been suggested to facilitate or power DNA release. Most dsDNA bacteriophages have mechanisms, such as glue proteins in epsilon 15 or chemical crosslinking of the capsid shell proteins as in HK97, to strengthen the capsid shell against this pressure. So how do the capsid proteins, the scaffolding proteins, the glue, and the portal interact in this system of virus assembly?

3.4.4.1 "True" T = 7 Capsid Organization

Structures of procapsids and mature capsids of dsDNA bacteriophages such as P22 (Prasad et al. 1993; Thuman-Commike et al. 1996; Jiang et al. 2003; Chang et al. 2006; Chen et al. 2011), ε15 (Jiang et al. 2006, 2008) and HK97 (Wikoff et al. 2000, 2006; Huang et al. 2011) have been well characterized. In these viruses, the icosahedral lattice is established according to the classical Casper and Klug quasi-equivalence theory, i.e., with 415 identical subunits arranged as 11 pentamers at the pentavalent positions and 60 hexamers at the hexavalent lattice points of the $T = 7l$ icosahedral lattice (Fig. 3.9). The true $T = 7$ symmetry is locally broken at one of the fivefold vertices because of the presence of the portal protein complex and sometimes a tail; as a result, there are only 11 pentamers instead of 12. The subunits at the hexavalent positions in the procapsids of these viruses show a skewed arrangement and only adopt a near sixfold symmetric organization in the mature capsids (Fig. 3.9a, b). Interestingly, as in the case of $T = 3$ viruses, which all exhibit a canonical jelly roll β-barrel structure, these viruses and other tailed bacteriophages (Baker et al. 2005; Fokine et al. 2005) also exhibit a common fold that was first described in the high-resolution crystallographic structure of HK97 and hence is called HK97-like fold (Wikoff et al. 2000, see also Chap. 15) (Fig. 3.9c). Unlike in the case of papovaviruses, in which the capsid protein is preformed into pentamers (one species), the capsid protein subunits in these viruses have to switch between hexameric and pentameric clustering on the $T = 7$ lattice.

3.4.4.2 Scaffolding Protein

To ensure accurate formation of the capsid shell, these viruses use an elaborate mechanism involving a scaffold which is either provided by a separate virally encoded protein as in the case of P22 (Fane

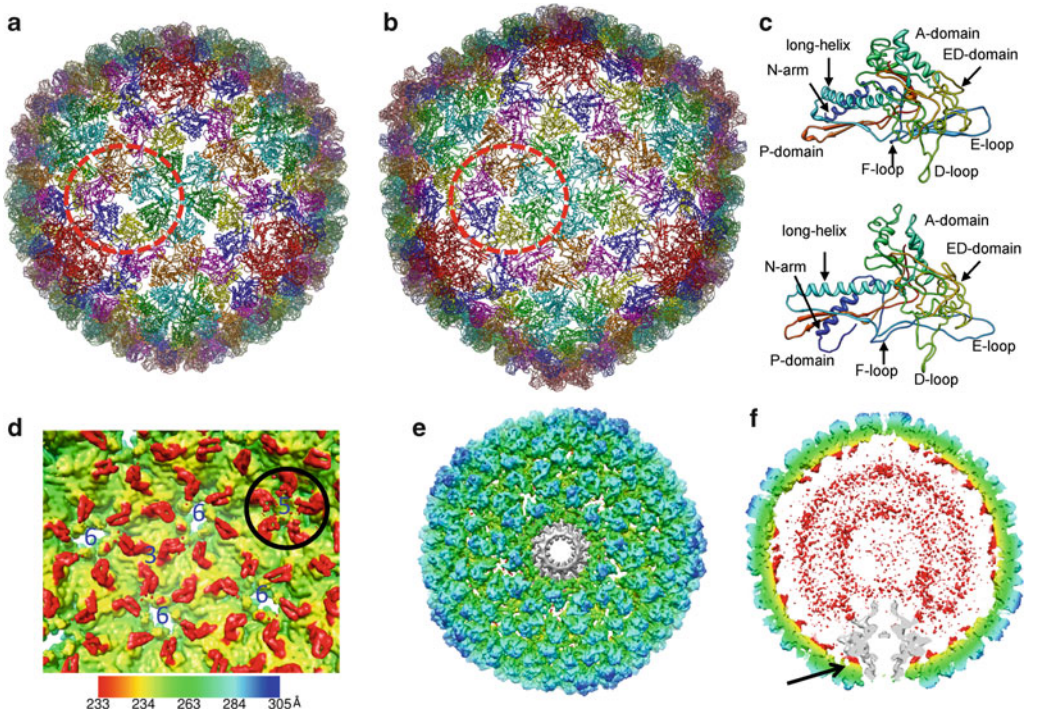


Fig. 3.9 Structural organization in the procapsid and mature capsid of P22. (**a**) Subunit packing in the procapsid showing the hexameric and pentameric clustering of the capsid protein subunits on a $T=7l$ lattice. The backbone structure of the subunits shown is derived from the ~4 Å cryo-EM structure. The subunits surrounding the fivefold axes are colored in *red*, and the six quasi-equivalent subunits at the hexavalent nodes (*circled* in *red*) are shown in different colors. Notice the spherical shape of the capsid, skewed clustering of the subunits around a hole at the hexavalent positions. These holes may be the exit points for the scaffolding proteins. (**b**) Mature capsid structure at ~4 Å determined using cryo-EM technique. The subunits are colored as in (**a**). Notice the angular shape, symmetric organization of the hexavalent subunits, and closure of the hole (*red circle*). (**c**) Conformational changes in the capsid subunit. *Above*: procapsid subunit. *Below*: Mature capsid subunit. The domains and the loops in the HK97-like fold are shown. (**d**) Inside surface of the procapsid showing the density due to scaffolding protein (*red*). (**e**) Asymmetric reconstruction of the procapsid, viewed along the 12-fold axis of the portal. (**f**) Cross-section showing the inward extension of the portal density. Figures from Donghua Chen and Wah Chiu

and Prevelige 2003, see also Chap. 14) or by a part of the capsid protein itself as in the case of HK97 (Huang et al. 2011). In P22, the scaffolding protein exits signaling for the maturation of the capsid, and then, it is recycled for the further rounds procapsid assembly. In the case HK97, the reordering of the N-terminal region of the capsid protein is suggested to provide a trigger for the maturation (Huang et al. 2011).

Recent cryo-EM reconstructions of P22 procapsid have provided some insights into the possible role of scaffolding proteins in directing the $T=7$ procapsid assembly (Parent et al. 2010a, b; Chen et al. 2011). In the reconstructions of the P22 procapsid, imposing icosahedral symmetry, the major portion of the scaffolding protein density is not clearly observed, suggesting that the majority of the scaffolding protein does not conform to the icosahedral symmetry of the capsid. However, the portion that interacts with the inside surface of the capsid shell is visible (Fig. 3.9d). These interactions are observed to be stronger with the hexavalent subunits than with the pentavalent subunits, suggesting that scaffolding protein may promote or stabilize the hexamer of the capsid protein relative to the pentamer. It is clear that the scaffolding proteins influence the icosahedral lattice because P22 mutants with altered or missing scaffolding proteins make a significant number of $T=4$ capsid shells with half the number of hexavalently disposed units, i.e., 30 versus 60

(Thuman-Commike et al. 1998). Thus, the scaffolding protein may influence the formation of the hexameric and pentameric clustering of the capsid protein subunits by altering the ratio of hexamers to pentamers during the assembly process.

3.4.4.3 The Portal

There is no evidence that the capsid proteins of P22 oligomerize into either hexamers or pentamers before being incorporated into the capsid shell. Thus, the shell appears to be built monomer by monomer, without the participation of preformed pentamers or hexamers. It is likely that the portal protein together with scaffolding protein guides the assembly of capsid protein into the correct shell. Visualization of the portal complex, because it is located at only one of the 12 fivefold vertices, requires reconstructions of the capsid structure without imposing icosahedral symmetry as was first done in the case of phi29 (Tao et al. 1998) and subsequently with several other dsDNA bacteriophages including P22 (Jiang et al. 2006; Chen et al. 2011). In the cryo-EM reconstructions of P22 procapsid, without imposing the icosahedral symmetry, the portal protein complex is clearly seen and sits as a dodecamer at one of the fivefold vertices (Chen et al. 2011) (Fig. 3.9e, f). Such a reconstruction shows that the portal interacts more directly with scaffolding protein than with the capsid shell in the procapsid consistent with the notion that scaffolding protein recruits the portal protein complex (Fane and Prevelige 2003). This suggests that the portal protein is a key participant in the capsid assembly (Chen et al. 2011). If the level of portal protein is kept well below that of the scaffolding or capsid proteins, the portal protein may nucleate the assembly of a capsid shell by its interactions with scaffolding and capsid shell proteins. This would in turn assure that there is only one portal per capsid, which is a requirement for proper DNA packaging. Capsids assembled in the absence of portal proteins are aberrant in their size, form, and/or symmetry.

3.4.4.4 Maturation and Expansion

During maturation of P22, the capsid protein undergoes a major conformational change, making the capsid shell thinner and the hexon interactions more symmetric. The shell becomes more angular from its round shape in the procapsid, is thinner by about 40 Å, and expands in diameter by about 100 Å (Prasad et al. 1993; Chen et al. 2011). The process of DNA packaging and concomitant release of the scaffolding proteins, through the small holes at the hexavalent positions of the procapsid, may trigger the conformational changes in the subunits and subunit contacts resulting in a dramatically expanded capsid. Similar expansion accompanied by large-scale conformational change upon maturation is also observed in HK97 and ε15 (Jiang et al. 2006; Wikoff et al. 2006). In the HK97, maturation is accompanied by the formation of an intersubunit isopeptide linkage that cross-links the entire capsid conferring stability to the capsid to withstand the pressure created by DNA packaging. In P22, which does not form a cross-linked capsid like HK97, strong protein–protein interactions among its capsid shell subunits appear to render sufficient structural rigidity in the mature virion (Parent et al. 2010a, b; Chen et al. 2011).

3.4.4.5 Glue Proteins

The nucleocapsid of herpesvirus, a dsDNA virus of eukaryotic origin with a distinctly different structural organization, nevertheless shares several characteristics with dsDNA bacteriophages (Heymann et al. 2003). It exhibits a $T = 16$ icosahedral structure (~1,250 Å in diameter) with pentamer and hexamer clustering of the major capsid protein VP5. 960 copies of VP5 forms 12 pentamers

and 150 ($10T-1$) hexamers as expected from the quasi-equivalent symmetry (Schrag et al. 1989; Zhou et al. 1994, 2000). In addition to VP5, capsid also consists of what are known as triplex proteins, VP19c and VP23 (in a stoichiometric ratio of 1:2), that are positioned at the local and strict threefold axes of the $T=16$ lattice. These triplexes function as glue holding together the surrounding VP5 capsomeres. Similar to dsDNA bacteriophages, capsid assembly is assisted by scaffolding protein which is proteolytically degraded prior to the packaging of the genomic DNA (Nicholson et al. 1994; Rixon et al. 1996). Recombinant baculovirus expression of VP5 and VP19c alone, i.e., in the absence of VP23 and the scaffolding protein, results in smaller-sized particles with $T=7$ symmetry suggesting the role of VP23 and the scaffolding protein in ensuring the correct capsid assembly (Saad et al. 1999). Another interesting similarity with dsDNA bacteriophages is that VP5 exhibits the HK97-like fold (Baker et al. 2003; Bowman et al. 2003). In addition to these components, as revealed by the electron cryo-tomographic reconstructions, the nucleocapsid has a unique fivefold vertex with a 12-fold symmetric portal for inserting the genomic dsDNA (Cardone et al. 2007; Chang et al. 2007; Deng et al. 2007). The nucleocapsid capsid also exhibits maturation-dependent morphological alterations (Heymann et al. 2003). These observations clearly indicate that DNA packaging mechanism in herpes virus resembles that in the tailed dsDNA bacteriophages.

Adenovirus, another dsDNA virus, represents more intricate and complex architecture (~1,000 Å in diameter) involving the arrangement of multiple proteins on a triangulated icosahedral lattice. It shows a different solution for the problem of pentamer and hexamer clustering on such a lattice. In this virus, the capsid organization is based on a pseudo $T=25$ lattice (Stewart et al. 1991; Liu et al. 2010; Reddy et al. 2010). Instead of the same protein forming a pentameric and hexameric clusters as in the case of dsDNA bacteriophages discussed above, two different proteins occupy the pentavalent and hexavalent positions on the $T=25$ lattice (Fig. 3.10a). The protein called penton base forms a penton at the 12 vertices incorporating a trimer of the fiber protein, and another protein called hexon occupy the 260 hexavalent positions on the $T=25$ lattice, however, as trimers. Crystallographic structures of penton (Zubieta et al. 2005), hexon (Roberts et al. 1986; Athappilly et al. 1994), and the fiber protein (van Raaij et al. 1999) have been determined. Previous cryo-EM studies provided some insights into the overall capsid organization in this complex virus (Stewart et al. 1991; Saban et al. 2006). Recently, the structure of the adenovirus capsid has been determined to near 3 Å resolution using X-ray crystallographic (Reddy et al. 2010) as well as cryo-EM techniques (Liu et al. 2010) providing a clearer picture of the intricate interactions between various components in the capsid organization (Fig. 3.10). The hexon protein, which forms stable trimers in solution, is incorporated in this oligomeric state into the capsid structure. Each hexon subunit exhibits an elaborate structure with two jelly roll β-barrels. In the hexon trimer, the disposition of these six β-barrels, two from each subunit, is such that it gives a pseudohexagonal contour to the trimer base appropriate for close packing of hexons at the hexavalent positions in the $T=25$ lattice. The pentons and hexons are held together in the capsid structure by an intricate network of glue (or cement) proteins (Fig. 3.10b). A similar pseudo $T=25$ capsid organization is also observed in PRD1, an enveloped dsDNA bacteriophage (Abrescia et al. 2004, 2008; Cockburn et al. 2004, see also Chap. 16). The P3 protein of PRD1 positioned at the hexavalent positions of the $T=25$ lattice also exhibits a similar "double β-barrel trimer" suggesting such a trimeric organization is evolutionarily conserved (Benson et al. 1999, 2002, 2004; Saren et al. 2005).

3.4.4.6 Cores

The dsRNA viruses particularly in the family Reoviridae such as rotavirus, bluetongue virus, and reovirus with 10–12 dsRNA genomic segments, which encode multiple structural proteins, exhibit even more elaborate and complex icosahedral capsid organization with multiple concentric capsid layers (Fig. 3.11) (Lawton et al. 2000; Jayaram et al. 2004; Harrison 2007). The complex structural

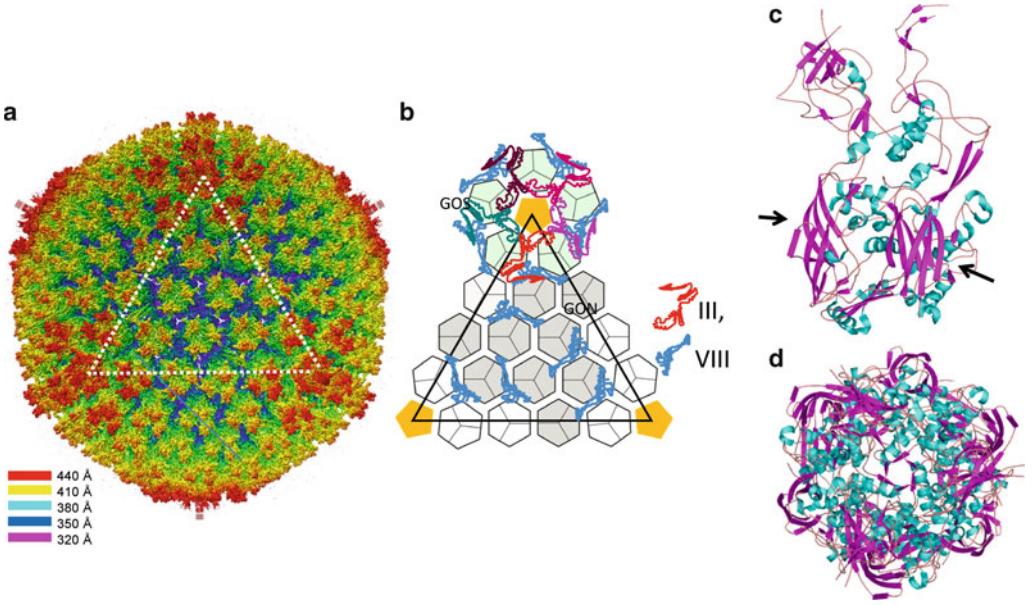


Fig. 3.10 Adenovirus capsid organization. (**a**) 3.4 Å cryo-EM structure of adenovirus capsid as viewed along the icosahedral threefold axis. One of the icosahedral facets is indicated by *dashed white lines*. The structure is radially colored according to the chart shown. (**b**) Schematic representation of structural organization of pentons, hexons, and the cement proteins (VIII, IIIA) in the $T=25$ (pseudo) icosahedral facet [same as indicated in (**a**)]. The hexon trimers are shown as *hexagons* and pentons as *pentagons* in *golden yellow*. The color coding for the cement proteins are shown in the side. The so-called GON (group of nine) hexons, because they remain associated following the capsid disassembly, are shaded in *gray*. The fiber protein which insets in to the penton is not observed in the cryo-EM structure as they are flexible. (**c**) Crystallographic structure of the hexon subunit. The orientation of the subunit structure is chosen such that top region is at the virion exterior. The structure is colored according to the secondary structural elements; α-helices in *cyan*, β-sheets in *pink*, and loops in *brown*. The radially oriented β-barrels are shown by *black arrows*. (**d**) Hexon trimer as viewed from the top, corresponding to the view of the trimer in the center of virion structure (**a**) along the icosahedral threefold axis. The structure is colored following the same scheme as in (**c**). The trimer has a striking hexagonal contour at its base, because of the orientation of the two β-barrels in each subunit, which is appropriate for its location at the 6-fold positions of the T=25 lattice. Fig. 3.10a, b from Dr. Hong Zhou

organization in these viruses appears to have evolved to compartmentalize the requirement of host cell interaction and the necessity to transcribe multiple genome segments within the capsid layers. Because the host cells do not have enzymatic machinery to convert dsRNA into mRNA, these viruses carry within the capsid interior of the enzymes required for transcribing the genome segments into mRNA and also capping the transcripts. It is to the advantage of the virus to carry out transcription endogenously not only to avoid any degradation of the genome by cellular nucleases but also to prevent cellular antiviral interferon response triggered by increased concentrations of dsRNA during replication, particularly in mammalian hosts.

One common theme in these dsRNA viruses is the assembly of the outer capsid layer(s), typically based on $T=13l$ icosahedral symmetry, and is assembled on the innermost layer that surrounds the dsRNA genome (see also Chap. 17). This innermost layer exhibits unusual icosahedral organization consisting of 120 subunits (forbidden "$T=2$") arranged as 60 asymmetric dimers on a $T=1$ icosahedral lattice (Lawton et al. 1997; Grimes et al. 1998; Reinisch et al. 2000; Chen et al. 2006) (Fig. 3.11e). Such an organization appears to be highly conserved in all the dsRNA viruses including dsRNA viruses of bacterial and fungal origins (Naitow et al. 2002; Ochoa et al. 2008), and the available structural data also indicate that the polypeptide folds of the proteins that form this layer are similar, despite lacking any noticeable sequence similarity.

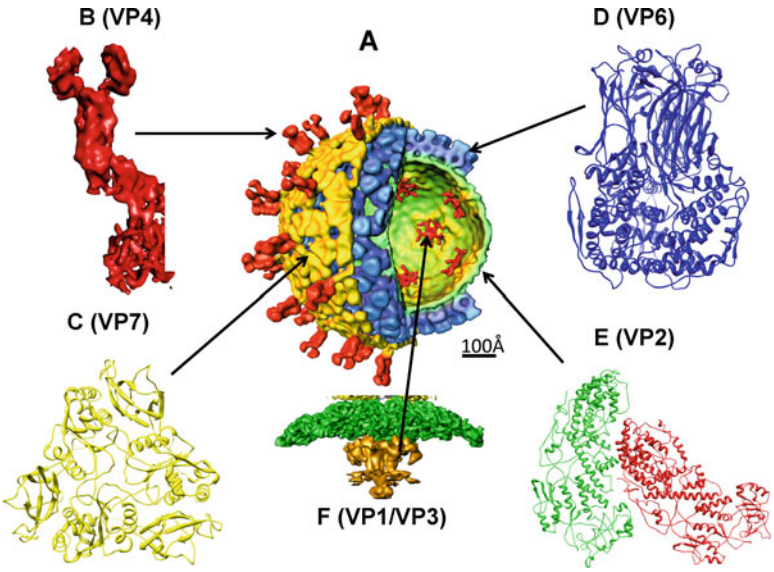


Fig. 3.11 Structure and location of various protein components in the triple-layered architecture of rotavirus are shown using a cutaway view of a lower-resolution cryo-EM structure of the TLP as the reference. (**a**) The mature rotavirus particle consisting of VP4 spikes (*red*) that emanate from the outer capsid layer, VP7 layer which exhibits a $T=13l$ icosahedral organization with 260 VP7 trimers located at all the icosahedral and local threefold axes (*yellow*), VP6 layer (*blue*), which also exhibits a $T=13$ icosahedral organization with 260 VP6 trimers, and the innermost VP2 layer consisting of 120 subunits of VP2 (*green*). The transcriptional enzymes VP1/VP3 anchored to the VP2 layer and projecting inward from the fivefold axes are shown in *red*. (**b**) A VP4 spike extracted from the cryo-EM map (Li et al. 2009). The foot domain is also indicated. (**c**) X-ray structure of VP7 trimer (PDB ID:3FMG, Aoki et al. 2009). (**d**) X-ray structure of VP6 trimer (PDB ID:1QHD, Mathieu et al. 2001). (**e**) Structure of the VP2 dimer that constitutes the icosahedral asymmetric unit of the innermost capsid layer (PDB ID:3KZ4, McClain et al. 2010) (**f**) Transcription enzymes VP1/VP3 (shown in *gold*) inside the VP2 layer in *green*

It is possible that this unique organization of the core capsid layer in these viruses has evolved to serve a dual purpose: to properly position the transcription enzyme complex and organize the genome to facilitate endogenous transcription. In many of these viruses, the virally encoded enzymes required for the transcription (RNA-dependent RNA polymerase) and capping intimately associate with this layer at the fivefold positions (Prasad et al. 1996; Zhang et al. 2003; Nason et al. 2004). One model is that pentamers of dimers of the subunits in the core layer associate along with the transcription enzyme complex, and 12 of these pentamers further associate to form the core layer with 120 subunits, which then serves as a platform for the assembly of the outer layers perhaps by sequential addition oligomeric (typically trimers) of capsid protein that constitutes the outer layer(s).

3.5 Helical Viruses

In addition to icosahedral symmetry that is commonly found in the spherical viruses, another symmetry that is prevalent among viruses is the helical symmetry. Many rod-shaped viruses such as viruses belonging to family Tobamoviruses (Namba and Stubbs 1986, see also Chap. 28), potyviruses (Kendall et al. 2008), rhabdoviruses (Ge et al. 2010), and nucleocapsids of several animal viruses such as Sendai viruses (Egelman et al. 1989) exhibit this kind of symmetry. In contrast to icosahedral symmetry which involves only rotational symmetry, helical symmetry involves both

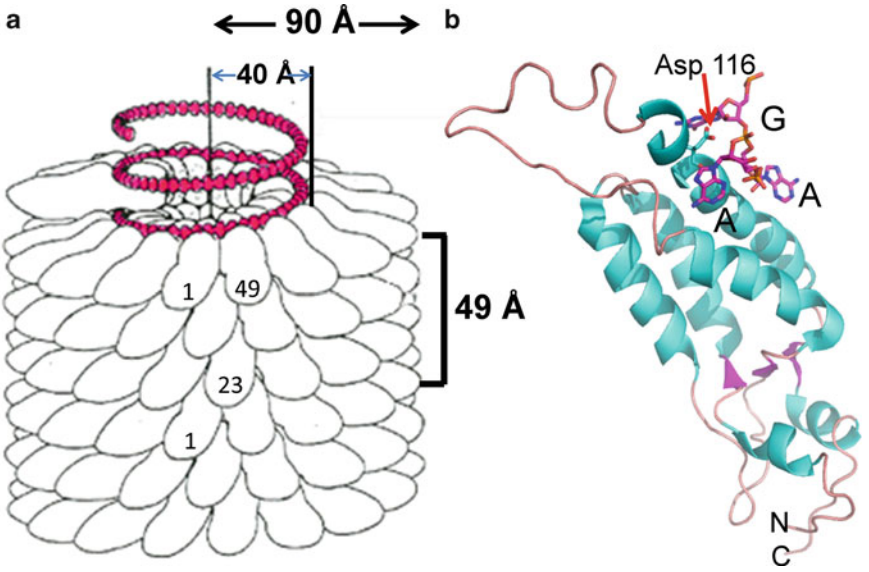


Fig. 3.12 The structure of TMV, an example of a helical virus. (**a**) Cartoon representation of the helical arrangement of the subunits in the TMV. The shoe-shaped capsid protein subunits wrap around the genomic RNA (*red*) following helical symmetry. Some of the subunits are numbered to indicate number of subunits in a turn of the helix. The radius of the helical assembly, pitch of the helix, along with inside radius at which protein interacts with the genomic RNA is indicated. (**b**) A cartoon representation of the crystallographic structure of the TMV capsid protein subunit with three nucleotides of the genomic RNA (PDB ID:2TMV, Namba et al. 1989). The N- and C-termini are denoted. The structure is colored according to the secondary structural elements (*cyan* – α-helices, *red* – β-strands, and *brown* – loops). The RNA bases are indicated along with the location of the residues Asp 116 of the capsid protein

rotational and translational components, which when combined, give a screw axis. Repeated application of rotation to a motif followed by translation along an axis gives rise to a structure with helical symmetry with a defined pitch (*P*). Helical structures are typically characterized by the radial location of the subunit with respect to the helix axis; the rotation per subunit, which is equivalent to the number of subunits per turn (*n*) in the helix; and the axial rise per subunit (*h*).

The best-characterized example of a helical virus is tobacco mosaic virus (TMV). It is a rod-shaped virus ~3,000 Å long and 180 Å in diameter, with a central hole of 40 Å in diameter. The structure of TMV has been determined to 2.8 Å resolution using X-ray fiber diffraction studies (Namba and Stubbs 1986; Namba et al. 1989) and most recently to a similar resolution using cryo-EM techniques (Ge and Hong Zhou 2011). The capsid protein of TMV forms a one-start, right-handed helix of pitch 23 Å, with 16-1/3 subunits in each turn (Fig. 3.12a). Interestingly, such a capsid organization leads to hexagonal close packing of the subunits, which is a common theme in many of icosahedral virus structures as discussed above. In icosahedral viruses, the encapsidated genome often does not obey the symmetry of the capsid; as a result, in the structural studies of these viruses which implicitly make use of the icosahedral symmetry, information about the structure of the genome and how it is organized is lost. However, in the case of TMV, the entire genome is well ordered and follows the helical symmetry of the capsid, thus providing details of not only how the capsid subunits interact with the genome but also how these interactions lead to virus assembly. The capsid subunits in the TMV structure wrap around the genomic RNA such that the RNA lies inside a groove, at a radius of 40 Å, between successive helical turns. Each subunit interacts with three nucleotides. The subunit structure is predominantly alpha-helical with a core consisting of a right-handed four antiparallel α-helix bundle (Fig. 3.12b). One of the helices from this bundle makes extensive contacts with the genomic RNA.

The interactions between the TMV capsid protein and the genomic RNA in general are nonspecific involving the basic residues of the protein and the phosphate groups of the RNA. One exception, however, is the anomalous repulsive interaction between the carboxylate group of Asp116 and a phosphate group of the RNA (Namba et al. 1989; Ge and Hong Zhou 2011) (Fig. 3.12b). Considering that TMV, and in general any viral assembly, has to assemble and disassemble during its infectious cycle, it is suggested that such a repulsive interaction, which may be required to maintain an energy balance, confers metastable nature to the TMV and functions as a trigger for driving viral disassembly (Namba et al. 1989; Culver et al. 1995; Stubbs 1999).

The assembly process in TMV has been studied extensively, and it serves as the best-characterized example of cocondensation of capsid protein and genomic RNA. In this process, the viral RNA interacts with a 20S aggregate, a two-turn helix of the capsid protein, and the assembly proceeds by addition of 20S aggregates through a highly cooperative process pulling the 5′ end of the RNA through the central hole of the growing TMV rod (Caspar and Namba 1990; Butler 1999; Klug 1999). It is suggested that a disorder-to-order transition of a loop in the capsid protein, analogous to conformational switching in the icosahedral viruses, that is induced by the binding of RNA may play an important role in this process (Namba et al. 1989; Culver et al. 1995). In the X-ray structure of the 20S aggregate, this particular loop is disordered, whereas in the TMV structure, it is ordered. The TMV assembly is initiated by the specific recognition of the sequence AAGAAGUCG in the viral RNA by the TMV capsid protein (Zimmern 1976; Butler 1999). The high-resolution structure of the fully assembled TMV has provided some insights in to how the capsid protein recognizes this sequence (Namba et al. 1989). Although the three RNA-binding sites in each subunit can accommodate any base, one of the binding sites is particularly suitable for G and allows favorable hydrogen bond interactions. In the initiation sequence, every third nucleotide being G thus may provide a strong discrimination for the higher affinity binding of the packaging signal over the rest of the sequence in which the XXG motif does not occur in phase with a statistically significant frequency.

3.6 Enveloped Viruses

During their morphogenesis, several viruses acquire a lipid envelope derived from a cellular organelle which remains part of their capsid organization. In some of the viruses such as influenza viruses, herpes viruses, coronaviruses, bunya viruses, and HIV, the lipid envelop is externally located and is studded by various viral proteins, whereas in others such as alphaviruses and flaviviruses, the lipid envelop is internally located underneath the outer proteinaceous capsid layer. With the exception of alphaviruses and flaviviruses, many of the enveloped viruses lack highly symmetric organization and are less amenable for high-resolution structural analysis. However, structures of the individual protein components of these enveloped viruses, e.g., hemagglutinin (Wilson et al. 1981; Bullough et al. 1994), neuraminidase (Varghese et al. 1983; Xu et al. 2008), and M2 protein of influenza virus (Acharya et al. 2010); glycoprotein of mouse hepatitis virus (Xu et al. 2004); gp120 and gp41 of retroviruses (Chan et al. 1997; Chen et al. 2005); envelop protein of a flavivirus (Rey et al. 1995; Rey 2003; Li et al. 2008); and most recently, E1/E2 complex of alphaviruses, have been well characterized (Li et al. 2010; Voss et al. 2010). These structures have provided significant insight into the mechanism of how the lipid bilayers in these viruses fuse with the membrane of the target cell (Rey 2006; Lamb and Jardetzky 2007; Harrison 2008). In addition, the highly symmetric parts of enveloped viruses such as the nucleocapsid of herpes virus that exhibit $T=16$ icosahedral organization (as discussed above) and the core of hepatitis B virus, which can form either a $T=3$ or a $T=4$ icosahedral structure, have been well characterized (Crowther et al. 1994; Conway et al. 1997; Wynne et al. 1999).

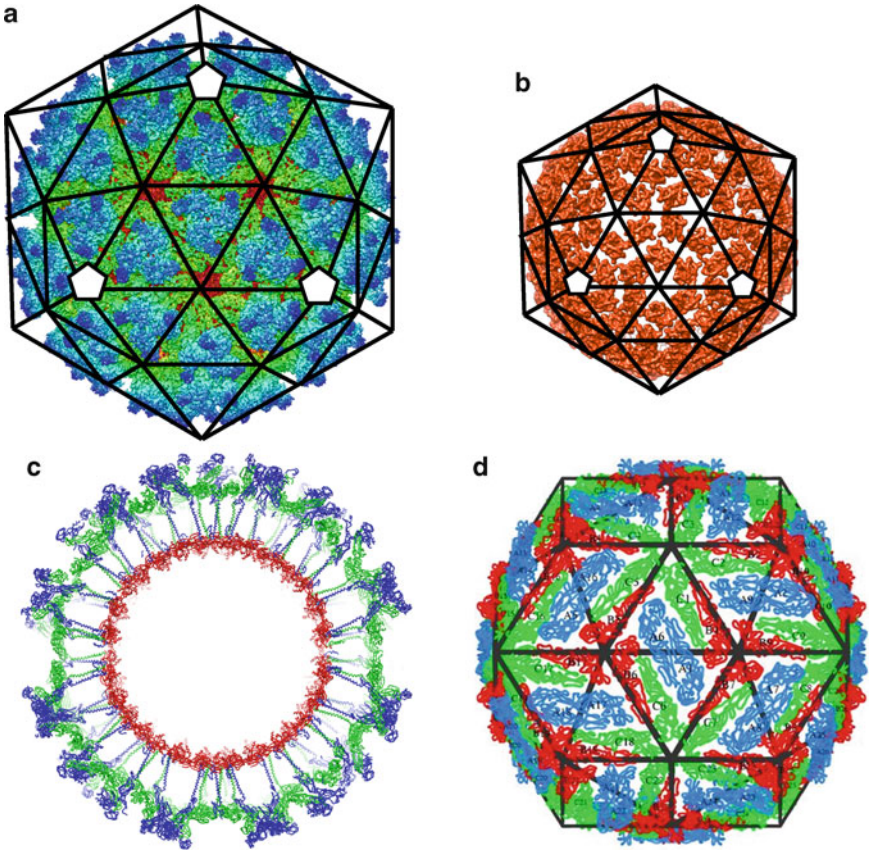


Fig. 3.13 Icosahedral organization in the enveloped viruses. (**a**) Cryo-EM structure of Venezuelan encephalitis virus (VEE), an alphavirus, determined to ~4.5 Å resolution showing the overall organization of the outer capsid composed of 80 trimers of E1 (*green*) and E2 (*blue*) heterodimers (Zhang et al. 2011). These trimers occupy local and strict threefold axes of the $T=4$ icosahedral lattice (*black lines*). (**b**) Structure of the VEE inner capsid extracted from the cryo-EM of the virion shown in (**a**). 240 subunits of the capsid protein are organized on a $T=4$ lattice (*black lines*) in register with the outer $T=4$ E1/E2 capsid layer. (**c**) An equatorial section showing the interactions between the outer E1/E2 proteins (*green* and *blue*) with the inner capsid protein (*red*) through the membrane bilayer. (**d**) Structural organization in the dengue virus, a flavivirus (obtained from VIPER, Reddy et al. 2001). The 180 copies of the E protein are organized as 90 dimers on the surface of the virion. The three subunits in the icosahedral asymmetric unit are colored in *blue*, *green*, and *red*. Despite having 180 subunits, as can be seen, the packing of the 90 dimers in a herringbone-like pattern is not quasi-equivalent and does not follow quasi-equivalent $T=3$ icosahedral lattice (shown in *black lines* for reference) (Fig. 3.13**a**–**c**, courtesy Corey Hryc and W. Chiu)

The only enveloped viruses that have been structurally characterized to high resolution are the internally enveloped alphaviruses such as Sindbis virus (Paredes et al. 1993, 1998; Zhang et al. 2002), Venezuelan encephalitis virus (Zhang et al. 2011), and Semliki Forest virus (Mancini et al. 2000) and flaviviruses such as dengue virus (Kuhn et al. 2002; Kaufmann et al. 2006; Pokidysheva et al. 2006; Li et al. 2008; Yu et al. 2008a, b). These viruses exhibit icosahedral organization. Alphaviruses consist of two concentric $T=4$ capsid layers that bracket the lipid bilayer (Figs. 3.13a, b). The outer layer is formed by heterotrimers of E1 and E2 glycoproteins, whereas the inner layer is formed by the core protein (Fig. 3.13b). The N-terminal transmembrane helices of the E1 and E2 protein subunits penetrate across the underlying lipid layer and interact one-to-one with the core protein subunits enabling proper registry of the outer and inner $T=4$ layers (Fig. 3.13c).

Although the subunit organization in the capsid layers of the alphaviruses is generally in accordance with the principles of quasi-equivalence theory, the capsid of flaviviruses presents an entirely novel organization (Kuhn et al. 2002). The flavivirus outer capsid, which sits above the lipid bilayer, is composed of 90 dimers of the major capsid protein, E glycoprotein, arranged as sets of three nearly parallel dimers that lie tangentially on the icosahedral surface (Fig. 3.13d). Although the capsid consists of 90 dimers, their arrangement does not conform to a classical $T=3$ quasi-equivalent lattice. This structure thus can be best described as a $T=1$ icosahedral structure with three molecules in the asymmetric unit, analogous to the situation in the core particles of rotavirus with 120 subunits which is described as having a $T=1$ structure with two molecules in the asymmetric unit. In addition to the E protein, flavivirus capsid also consists of M protein whose precise location is not definitively assigned. In contrast to the alphaviruses, which have well-organized core structure, the nucleocapsid of the flavivirus formed by the C protein does not exhibit any ordered organization.

3.7 Conclusion

The quasi-equivalence theory proposed almost half a century ago has been remarkably useful in describing icosahedral virus structure. The generality of its predictions arises from the simplicity afforded by the assumption that groups of subunits packing in a plane are energetically favored to have six neighbors (i.e., are hexagonally close-packed) and that curvature can be generated by introducing nodes (vertices) with only five such neighbors. However, such generality and adaptability can come at the cost of specificity. The propensity for subunits to form quasi-equivalent interactions leading to a wrong (usually smaller and simpler) final capsid structure indicates that more information is sometimes required. So we observe that in some viruses with $T=7$ symmetry, such as P22, scaffolding proteins are used either as a template core around which a proper-sized capsid can form, or, more subtly, to control the relative proportion of subunits which adopt hexameric interactions to those which form pentamers. This idea of altering the stability of one conformational form over another is also exemplified in the RNA viruses, where the RNA plays a role in stabilizing capsid proteins in the proper ratio of conformations. In the members of *Reoviridae*, the inner core layer forms a simple $T=1$ "permanent scaffold" from 60 dimers, upon which the $T=13$ outer layers are built. In adenovirus and herpesvirus, the role of scaffolding is augmented by the incorporation of accessory proteins in the capsid shell, which also appear to function to influence the curvature, and therefore the triangulation number of the capsid shell. Finally, the tendency for hexagonal close packing to be a controlling influence in virus assembly appears to be so robust that in the case of polyomavirus, where pentamers seem to be the only oligomeric species present, pentamers come to occupy the hexavalent positions. The exceptions to the quasi-equivalence theory prove the rule.

Acknowledgments We acknowledge the support from NIH grants R37AI36040 (BVVP), PO1AI057788 (BVVP), P41RR02250 (MFS) and a grant from Robert Welch Foundation (Q1279) to BVVP. We are grateful to Donghua Chen, Corey Hryc, Liya Hu, Wah Chiu, and Hong Zhou for the help in the figures.

References

Abad-Zapatero C, Abdel-Meguid SS, Johnson JE, Leslie AG, Rayment I, Rossmann MG et al (1980) Structure of southern bean mosaic virus at 2.8 A resolution. Nature 286:33–39

Abrescia NG, Cockburn JJ, Grimes JM, Sutton GC, Diprose JM, Butcher SJ et al (2004) Insights into assembly from structural analysis of bacteriophage PRD1. Nature 432:68–74

Abrescia NG, Grimes JM, Kivela HM, Assenberg R, Sutton GC, Butcher SJ et al (2008) Insights into virus evolution and membrane biogenesis from the structure of the marine lipid-containing bacteriophage PM2. Mol Cell 31:749–761

Acharya R, Fry E, Stuart D, Fox G, Rowlands D, Brown F (1989) The three-dimensional structure of foot-and-mouth disease virus at 2.9 A resolution. Nature 337:709–716

Acharya R, Carnevale V, Fiorin G, Levine BG, Polishchuk AL, Balannik V et al (2010) Structure and mechanism of proton transport through the transmembrane tetrameric M2 protein bundle of the influenza A virus. Proc Natl Acad Sci USA 107:15075–15080

Aoki ST, Settembre EC, Trask SD, Greenberg HB, Harrison SC, Dormitzer PR (2009) Structure of rotavirus outer-layer protein VP7 bound with a neutralizing Fab. Science 324:1444–1447

Athappilly FK, Murali R, Rux JJ, Cai Z, Burnett RM (1994) The refined crystal structure of hexon, the major coat protein of adenovirus type 2, at 2.9 A resolution. J Mol Biol 242:430–455

Baker ML, Jiang W, Bowman BR, Zhou ZH, Quiocho FA, Rixon FJ et al (2003) Architecture of the herpes simplex virus major capsid protein derived from structural bioinformatics. J Mol Biol 331:447–456

Baker ML, Jiang W, Rixon FJ, Chiu W (2005) Common ancestry of herpesviruses and tailed DNA bacteriophages. J Virol 79:14967–14970

Baker ML, Zhang J, Ludtke SJ, Chiu W (2010) Cryo-EM of macromolecular assemblies at near-atomic resolution. Nat Protoc 5:1697–1708

Ban N, Larson SB, McPherson A (1995) Structural comparison of the plant satellite viruses. Virology 214:571–583

Belnap DM, McDermott BM Jr, Filman DJ, Cheng N, Trus BL, Zuccola HJ et al (2000) Three-dimensional structure of poliovirus receptor bound to poliovirus. Proc Natl Acad Sci USA 97:73–78

Benevides JM, Juuti JT, Tuma R, Bamford DH, Thomas GJ Jr (2002) Characterization of subunit-specific interactions in a double-stranded RNA virus: Raman difference spectroscopy of the phi6 procapsid. Biochemistry 41:11946–11953

Benson SD, Bamford JK, Bamford DH, Burnett RM (1999) Viral evolution revealed by bacteriophage PRD1 and human adenovirus coat protein structures. Cell 98:825–833

Benson SD, Bamford JK, Bamford DH, Burnett RM (2002) The X-ray crystal structure of P3, the major coat protein of the lipid-containing bacteriophage PRD1, at 1.65 A resolution. Acta Crystallogr D Biol Crystallogr 58:39–59

Benson SD, Bamford JK, Bamford DH, Burnett RM (2004) Does common architecture reveal a viral lineage spanning all three domains of life? Mol Cell 16:673–685

Bentley GA, Lewit-Bentley A, Liljas L, Skoglund U, Roth M, Unge T (1987) Structure of RNA in satellite tobacco necrosis virus. A low resolution neutron diffraction study using $1H_2O/2H_2O$ solvent contrast variation. J Mol Biol 194:129–141

Berger B, Shor PW, Tucker-Kellogg L, King J (1994) Local rule-based theory of virus shell assembly. Proc Natl Acad Sci USA 91:7732–7736

Bertolotti-Ciarlet A, White LJ, Chen R, Prasad BV, Estes MK (2002) Structural requirements for the assembly of Norwalk virus-like particles. J Virol 76:4044–4055

Bottcher B, Wynne SA, Crowther RA (1997) Determination of the fold of the core protein of hepatitis B virus by electron cryomicroscopy. Nature 386:88–91

Bowman BR, Baker ML, Rixon FJ, Chiu W, Quiocho FA (2003) Structure of the herpesvirus major capsid protein. EMBO J 22:757–765

Brenner S, Horne RW (1959) A negative staining method for high resolution electron microscopy of viruses. Biochim Biophys Acta 34:103–110

Bullough PA, Hughson FM, Skehel JJ, Wiley DC (1994) Structure of influenza haemagglutinin at the pH of membrane fusion. Nature 371:37–43

Butler PJ (1999) Self-assembly of tobacco mosaic virus: the role of an intermediate aggregate in generating both specificity and speed. Philos Trans R Soc Lond B Biol Sci 354:537–550

Cardone G, Winkler DC, Trus BL, Cheng N, Heuser JE, Newcomb WW et al (2007) Visualization of the herpes simplex virus portal in situ by cryo-electron tomography. Virology 361:426–434

Caspar DL (1956) Structure of bushy stunt virus. Nature 177:475–476

Caspar DL, Klug A (1962) Physical principles in the construction of regular viruses. Cold Spring Harb Symp Quant Biol 27:1–24

Caspar DL, Namba K (1990) Switching in the self-assembly of tobacco mosaic virus. Adv Biophys 26:157–185

Chan DC, Fass D, Berger JM, Kim PS (1997) Core structure of gp41 from the HIV envelope glycoprotein. Cell 89:263–273

Chang J, Weigele P, King J, Chiu W, Jiang W (2006) Cryo-EM asymmetric reconstruction of bacteriophage P22 reveals organization of its DNA packaging and infecting machinery. Structure 14:1073–1082

Chang JT, Schmid MF, Rixon FJ, Chiu W (2007) Electron cryotomography reveals the portal in the herpesvirus capsid. J Virol 81:2065–2068

Chen ZG, Stauffacher C, Li Y, Schmidt T, Bomu W, Kamer G et al (1989) Protein-RNA interactions in an icosahedral virus at 3.0 A resolution. Science 245:154–159

Chen B, Vogan EM, Gong H, Skehel JJ, Wiley DC, Harrison SC (2005) Structure of an unliganded simian immunodeficiency virus gp120 core. Nature 433:834–841

Chen R, Neill JD, Estes MK, Prasad BV (2006) X-ray structure of a native calicivirus: structural insights into antigenic diversity and host specificity. Proc Natl Acad Sci USA 103:8048–8053
Chen DH, Baker ML, Hryc CF, DiMaio F, Jakana J, Wu W et al (2011) Structural basis for scaffolding-mediated assembly and maturation of a dsDNA virus. Proc Natl Acad Sci USA 108:1355–1360
Cockburn JJ, Abrescia NG, Grimes JM, Sutton GC, Diprose JM, Benevides JM et al (2004) Membrane structure and interactions with protein and DNA in bacteriophage PRD1. Nature 432:122–125
Conway JF, Cheng N, Zlotnick A, Wingfield PT, Stahl SJ, Steven AC (1997) Visualization of a 4-helix bundle in the hepatitis B virus capsid by cryo-electron microscopy. Nature 386:91–94
Conway JF, Wikoff WR, Cheng N, Duda RL, Hendrix RW, Johnson JE et al (2001) Virus maturation involving large subunit rotations and local refolding. Science 292:744–748
Crick FH, Watson JD (1956) Structure of small viruses. Nature 177:473–475
Crick FHC, Watson JD (1957) Virus structure: general principles. In: Wolstenholme GEW, Millar ECP (eds) CIBA foundation symposium on the nature of viruses. Little Brown and Co, Boston
Crowther, RA (2010) From envelops to atoms: The remarkable progress of biological electron microscopy. Advances in Protein Chemistry and Structural Biology Vol 81 "Recent Advances in Electron cryomicroscopy" Part A, (eds, Ludtke S, and Prasad, BVV), pp 2–33.
Crowther RA, Amos LA, Finch JT, De Rosier DJ, Klug A (1970) Three dimensional reconstructions of spherical viruses by fourier synthesis from electron micrographs. Nature 226:421–425
Crowther RA, Kiselev NA, Bottcher B, Berriman JA, Borisova GP, Ose V et al (1994) Three-dimensional structure of hepatitis B virus core particles determined by electron cryomicroscopy. Cell 77:943–950
Culver JN, Dawson WO, Plonk K, Stubbs G (1995) Site-directed mutagenesis confirms the involvement of carboxylate groups in the disassembly of tobacco mosaic virus. Virology 206:724–730
Deng B, O'Connor CM, Kedes DH, Zhou ZH (2007) Direct visualization of the putative portal in the Kaposi's sarcoma-associated herpesvirus capsid by cryoelectron tomography. J Virol 81:3640–3644
Dong XF, Natarajan P, Tihova M, Johnson JE, Schneemann A (1998) Particle polymorphism caused by deletion of a peptide molecular switch in a quasiequivalent icosahedral virus. J Virol 72:6024–6033
Dormitzer PR, Nason EB, Prasad BV, Harrison SC (2004) Structural rearrangements in the membrane penetration protein of a non-enveloped virus. Nature 430:1053–1058
Dubochet J, Adrian M, Chang JJ, Homo JC, Lepault J, McDowall AW et al (1988) Cryo-electron microscopy of vitrified specimens. Q Rev Biophys 21:129–228
Egelman EH, Wu SS, Amrein M, Portner A, Murti G (1989) The Sendai virus nucleocapsid exists in at least four different helical states. J Virol 63:2233–2243
Erickson JW, Silva AM, Murthy MR, Fita I, Rossmann MG (1985) The structure of a T = 1 icosahedral empty particle from southern bean mosaic virus. Science 229:625–629
Fane BA, Prevelige PE (2003) Mechanism of scaffold-assisted viral assembly. Adv Protein Chem 64:259–299
Fisher AJ, Johnson JE (1993) Ordered duplex RNA controls capsid architecture in an icosahedral animal virus. Nature 361:176–179
Fokine A, Chipman PR, Leiman PG, Mesyanzhinov VV, Rao VB, Rossmann MG (2004) Molecular architecture of the prolate head of bacteriophage T4. Proc Natl Acad Sci USA 101:6003–6008
Fokine A, Leiman PG, Shneider MM, Ahvazi B, Boeshans KM, Steven AC et al (2005) Structural and functional similarities between the capsid proteins of bacteriophages T4 and HK97 point to a common ancestry. Proc Natl Acad Sci USA 102:7163–7168
Gan L, Speir JA, Conway JF, Lander G, Cheng N, Firek BA et al (2006) Capsid conformational sampling in HK97 maturation visualized by X-ray crystallography and cryo-EM. Structure 14:1655–1665
Ge P, Hong Zhou Z (2011) Hydrogen-bonding networks and RNA bases revealed by cryo electron microscopy suggest a triggering mechanism for calcium switches. Proc Natl Acad Sci USA 108:9637–9642
Ge P, Tsao J, Schein S, Green TJ, Luo M, Zhou ZH (2010) Cryo-EM model of the bullet-shaped vesicular stomatitis virus. Science 327:689–693
Green EM, Horne RW, Matthews RE (1956) Electron microscope observations of periodicities in the surface structure of tobacco mosaic virus. Nature 178:635–636
Grigorieff N, Harrison SC (2011) Near-atomic resolution reconstructions of icosahedral viruses from electron cryomicroscopy. Curr Opin Struct Biol 21:265–273
Grimes JM, Jakana J, Ghosh M, Basak AK, Roy P, Chiu W et al (1997) An atomic model of the outer layer of the bluetongue virus core derived from X-ray crystallography and electron cryomicroscopy. Structure 5:885–893
Grimes JM, Burroughs JN, Gouet P, Diprose JM, Malby R, Zientara S et al (1998) The atomic structure of the bluetongue virus core. Nature 395:470–478
Harrison SE (2007) Principles of virus structure. Lippincott Williams and Wilkins, Philadelphia, PA
Harrison SC (2008) Viral membrane fusion. Nat Struct Mol Biol 15:690–698
Harrison SC, Olson AJ, Schutt CE, Winkler FK, Bricogne G (1978) Tomato bushy stunt virus at 2.9 A resolution. Nature 276:368–373

Heymann JB, Cheng N, Newcomb WW, Trus BL, Brown JC, Steven AC (2003) Dynamics of herpes simplex virus capsid maturation visualized by time-lapse cryo-electron microscopy. Nat Struct Biol 10:334–341
Hogle JM, Chow M, Filman DJ (1985) Three-dimensional structure of poliovirus at 2.9 A resolution. Science 229:1358–1365
Hogle JM, Maeda A, Harrison SC (1986) Structure and assembly of turnip crinkle virus. I. X-ray crystallographic structure analysis at 3.2 A resolution. J Mol Biol 191:625–638
Horne RW, Wildy P (1962) Recent studies on the fine structure of viruses by electron microscopy, using negative-staining techniques. Br Med Bull 18:199–204
Horne RW, Wildy P (1979) An historical account of the development and applications of the negative staining technique to the electron microscopy of viruses. J Microsc 117:103–122
Huang RK, Khayat R, Lee KK, Gertsman I, Duda RL, Hendrix RW et al (2011) The prohead-i structure of bacteriophage HK97: implications for scaffold-mediated control of particle assembly and maturation. J Mol Biol 408:541–554
Ilag LL, Olson NH, Dokland T, Music CL, Cheng RH, Bowen Z et al (1995) DNA packaging intermediates of bacteriophage phi X174. Structure 3:353–363
Jayaram H, Estes MK, Prasad BV (2004) Emerging themes in rotavirus cell entry, genome organization, transcription and replication. Virus Res 101:67–81
Jiang W, Li Z, Zhang Z, Baker ML, Prevelige PE Jr, Chiu W (2003) Coat protein fold and maturation transition of bacteriophage P22 seen at subnanometer resolutions. Nat Struct Biol 10:131–135
Jiang W, Chang J, Jakana J, Weigele P, King J, Chiu W (2006) Structure of epsilon15 bacteriophage reveals genome organization and DNA packaging/injection apparatus. Nature 439:612–616
Jiang W, Baker ML, Jakana J, Weigele PR, King J, Chiu W (2008) Backbone structure of the infectious epsilon15 virus capsid revealed by electron cryomicroscopy. Nature 451:1130–1134
Johnson JE, Speir JA (1997) Quasi-equivalent viruses: a paradigm for protein assemblies. J Mol Biol 269:665–675
Kaufmann B, Nybakken GE, Chipman PR, Zhang W, Diamond MS, Fremont DH et al (2006) West Nile virus in complex with the Fab fragment of a neutralizing monoclonal antibody. Proc Natl Acad Sci USA 103: 12400–12404
Kendall A, McDonald M, Bian W, Bowles T, Baumgarten SC, Shi J et al (2008) Structure of flexible filamentous plant viruses. J Virol 82:9546–9554
Klug A (1999) The tobacco mosaic virus particle: structure and assembly. Philos Trans R Soc Lond B Biol Sci 354:531–535
Klug A, Caspar DL (1960) The structure of small viruses. Adv Virus Res 7:225–325
Klug A, Finch JT (1968) Structure of viruses of the papilloma-polyoma type. IV. Analysis of tilting experiments in the electron microscope. J Mol Biol 31:1–12
Klug A, Finch JT, Franklin RE (1957) The structure of turnip yellow mosaic virus; x-ray diffraction studies. Biochim Biophys Acta 25:242–252
Knapek E, Dubochet J (1980) Beam damage to organic material is considerably reduced in cryo-electron microscopy. J Mol Biol 141:147–161
Kuhn RJ, Zhang W, Rossmann MG, Pletnev SV, Corver J, Lenches E et al (2002) Structure of dengue virus: implications for flavivirus organization, maturation, and fusion. Cell 108:717–725
Lamb RA, Jardetzky TS (2007) Structural basis of viral invasion: lessons from paramyxovirus F. Curr Opin Struct Biol 17:427–436
Larson SB, Koszelak S, Day J, Greenwood A, Dodds JA, McPherson A (1993) Double-helical RNA in satellite tobacco mosaic virus. Nature 361:179–182
Lawton JA, Zeng CQ, Mukherjee SK, Cohen J, Estes MK, Prasad BV (1997) Three-dimensional structural analysis of recombinant rotavirus-like particles with intact and amino-terminal-deleted VP2: implications for the architecture of the VP2 capsid layer. J Virol 71:7353–7360
Lawton JA, Estes MK, Prasad BV (2000) Mechanism of genome transcription in segmented dsRNA viruses. Adv Virus Res 55:185–229
Li L, Lok SM, Yu IM, Zhang Y, Kuhn RJ, Chen J et al (2008) The flavivirus precursor membrane-envelope protein complex: structure and maturation. Science 319:1830–1834
Li Z, Baker ML, Jiang W, Estes MK, Prasad BV (2009) Rotavirus architecture at subnanometer resolution. J Virol 83:1754–1766
Li L, Jose J, Xiang Y, Kuhn RJ, Rossmann MG (2010) Structural changes of envelope proteins during alphavirus fusion. Nature 468:705–708
Liddington RC, Yan Y, Moulai J, Sahli R, Benjamin TL, Harrison SC (1991) Structure of simian virus 40 at 3.8-A resolution. Nature 354:278–284
Liljas L, Unge T, Jones TA, Fridborg K, Lovgren S, Skoglund U et al (1982) Structure of satellite tobacco necrosis virus at 3.0 A resolution. J Mol Biol 159:93–108
Lin T, Chen Z, Usha R, Stauffacher CV, Dai JB, Schmidt T et al (1999) The refined crystal structure of cowpea mosaic virus at 2.8 A resolution. Virology 265:20–34

Liu H, Jin L, Koh SB, Atanasov I, Schein S, Wu L et al (2010) Atomic structure of human adenovirus by cryo-EM reveals interactions among protein networks. Science 329:1038–1043
Luo M, Vriend G, Kamer G, Minor I, Arnold E, Rossmann MG et al (1987) The atomic structure of Mengo virus at 3.0 A resolution. Science 235:182–191
Mancini EJ, Clarke M, Gowen BE, Rutten T, Fuller SD (2000) Cryo-electron microscopy reveals the functional organization of an enveloped virus, Semliki Forest virus. Mol Cell 5:255–266
Martin CS, Burnett RM, de Haas F, Heinkel R, Rutten T, Fuller SD et al (2001) Combined EM/X-ray imaging yields a quasi-atomic model of the adenovirus-related bacteriophage PRD1 and shows key capsid and membrane interactions. Structure 9:917–930
Mathieu M, Petitpas I, Navaza J, Lepault J, Kohli E, Pothier P et al (2001) Atomic structure of the major capsid protein of rotavirus: implications for the architecture of the virion. EMBO J 20:1485–1497
McClain B, Settembre E, Temple BR, Bellamy AR, Harrison SC (2010) X-ray crystal structure of the rotavirus inner capsid particle at 3.8 A resolution. J Mol Biol 397:587–599
Moody MF (1999) Geometry of phage head construction. J Mol Biol 293:401–433
Mukherjee S, Abd-El-Latif M, Bronstein M, Ben-nun-Shaul O, Kler S et al (2007) High Cooperativity of the SV40 Major Capsid Protein VP1 in Virus Assembly. PLoS ONE 2(8): e765. doi:10.1371/journal.pone.0000765
Naitow H, Tang J, Canady M, Wickner RB, Johnson JE (2002) L-A virus at 3.4 A resolution reveals particle architecture and mRNA decapping mechanism. Nat Struct Biol 9:725–728
Namba K, Stubbs G (1986) Structure of tobacco mosaic virus at 3.6 A resolution: implications for assembly. Science 231:1401–1406
Namba K, Pattanayek R, Stubbs G (1989) Visualization of protein-nucleic acid interactions in a virus. Refined structure of intact tobacco mosaic virus at 2.9 A resolution by X-ray fiber diffraction. J Mol Biol 208:307–325
Nason EL, Wetzel JD, Mukherjee SK, Barton ES, Prasad BV, Dermody TS (2001) A monoclonal antibody specific for reovirus outer-capsid protein sigma3 inhibits sigma1-mediated hemagglutination by steric hindrance. J Virol 75:6625–6634
Nason EL, Rothagel R, Mukherjee SK, Kar AK, Forzan M, Prasad BV et al (2004) Interactions between the inner and outer capsids of bluetongue virus. J Virol 78:8059–8067
Nicholson P, Addison C, Cross AM, Kennard J, Preston VG, Rixon FJ (1994) Localization of the herpes simplex virus type 1 major capsid protein VP5 to the cell nucleus requires the abundant scaffolding protein VP22a. J Gen Virol 75(Pt 5):1091–1099
Ochoa WF, Havens WM, Sinkovits RS, Nibert ML, Ghabrial SA, Baker TS (2008) Partitivirus structure reveals a 120-subunit, helix-rich capsid with distinctive surface arches formed by quasisymmetric coat-protein dimers. Structure 16:776–786
Ossiboff RJ, Zhou Y, Lightfoot PJ, Prasad BV, Parker JS (2010) Conformational changes in the capsid of a calicivirus upon interaction with its functional receptor. J Virol 84:5550–5564
Paredes AM, Brown DT, Rothnagel R, Chiu W, Schoepp RJ, Johnston RE et al (1993) Three-dimensional structure of a membrane-containing virus. Proc Natl Acad Sci USA 90:9095–9099
Paredes AM, Heidner H, Thuman-Commike P, Prasad BV, Johnston RE, Chiu W (1998) Structural localization of the E3 glycoprotein in attenuated Sindbis virus mutants. J Virol 72:1534–1541
Parent KN, Khayat R, Tu LH, Suhanovsky MM, Cortines JR, Teschke CM et al (2010a) P22 coat protein structures reveal a novel mechanism for capsid maturation: stability without auxiliary proteins or chemical crosslinks. Structure 18:390–401
Parent KN, Sinkovits RS, Suhanovsky MM, Teschke CM, Egelman EH, Baker TS (2010b) Cryo-reconstructions of P22 polyheads suggest that phage assembly is nucleated by trimeric interactions among coat proteins. Phys Biol 7:045004
Pokidysheva E, Zhang Y, Battisti AJ, Bator-Kelly CM, Chipman PR, Xiao C et al (2006) Cryo-EM reconstruction of dengue virus in complex with the carbohydrate recognition domain of DC-SIGN. Cell 124:485–493
Prasad BV, Prevelige PE (2003) Viral genome organization. Adv Protein Chem 64:219–258
Prasad BV, Prevelige PE, Marietta E, Chen RO, Thomas D, King J et al (1993) Three-dimensional transformation of capsids associated with genome packaging in a bacterial virus. J Mol Biol 231:65–74
Prasad BV, Rothnagel R, Zeng CQ, Jakana J, Lawton JA, Chiu W et al (1996) Visualization of ordered genomic RNA and localization of transcriptional complexes in rotavirus. Nature 382:471–473
Prasad BV, Hardy ME, Dokland T, Bella J, Rossmann MG, Estes MK (1999) X-ray crystallographic structure of the Norwalk virus capsid. Science 286:287–290
Rao VB, Black LW (2010) Structure and assembly of bacteriophage T4 head. Virol J 7:356
Reddy VS, Natarajan P, Okerberg B, Li K, Damodaran KV, Morton RT et al (2001) Virus Particle Explorer (VIPER), a website for virus capsid structures and their computational analyses. J Virol 75:11943–11947
Reddy VS, Natchiar SK, Stewart PL, Nemerow GR (2010) Crystal structure of human adenovirus at 3.5 A resolution. Science 329:1071–1075
Reinisch KM, Nibert ML, Harrison SC (2000) Structure of the reovirus core at 3.6 A resolution. Nature 404:960–967

Rey FA (2003) Dengue virus envelope glycoprotein structure: new insight into its interactions during viral entry. Proc Natl Acad Sci USA 100:6899–6901
Rey FA (2006) Molecular gymnastics at the herpesvirus surface. EMBO Rep 7:1000–1005
Rey FA, Heinz FX, Mandl C, Kunz C, Harrison SC (1995) The envelope glycoprotein from tick-borne encephalitis virus at 2 A resolution. Nature 375:291–298
Rixon FJ, Addison C, McGregor A, Macnab SJ, Nicholson P, Preston VG et al (1996) Multiple interactions control the intracellular localization of the herpes simplex virus type 1 capsid proteins. J Gen Virol 77(Pt 9):2251–2260
Roberts MM, White JL, Grutter MG, Burnett RM (1986) Three-dimensional structure of the adenovirus major coat protein hexon. Science 232:1148–1151
Rossmann MG, Johnson JE (1989) Icosahedral RNA virus structure. Annu Rev Biochem 58:533–573
Rossmann MG, Arnold E, Erickson JW, Frankenberger EA, Griffith JP, Hecht HJ et al (1985) Structure of a human common cold virus and functional relationship to other picornaviruses. Nature 317:145–153
Rossmann MG, Olson NH, Kolatkar PR, Oliveira MA, Cheng RH, Greve JM et al (1994) Crystallographic and cryo EM analysis of virion-receptor interactions. Arch Virol Suppl 9:531–541
Saad A, Zhou ZH, Jakana J, Chiu W, Rixon FJ (1999) Roles of triplex and scaffolding proteins in herpes simplex virus type 1 capsid formation suggested by structures of recombinant particles. J Virol 73:6821–6830
Saban SD, Silvestry M, Nemerow GR, Stewart PL (2006) Visualization of alpha-helices in a 6-angstrom resolution cryoelectron microscopy structure of adenovirus allows refinement of capsid protein assignments. J Virol 80: 12049–12059
Saren AM, Ravantti JJ, Benson SD, Burnett RM, Paulin L, Bamford DH et al (2005) A snapshot of viral evolution from genome analysis of the tectiviridae family. J Mol Biol 350:427–440
Schrag JD, Prasad BV, Rixon FJ, Chiu W (1989) Three-dimensional structure of the HSV1 nucleocapsid. Cell 56:651–660
Settembre EC, Chen JZ, Dormitzer PR, Grigorieff N, Harrison SC (2011) Atomic model of an infectious rotavirus particle. EMBO J 30:408–416
Shoemaker GK, van Duijn E, Crawford SE, Uetrecht C, Baclayon M, Roos WH et al (2010) Norwalk virus assembly and stability monitored by mass spectrometry. Mol Cell Proteomics 9:1742–1751
Smith TJ, Chase ES, Schmidt TJ, Olson NH, Baker TS (1996) Neutralizing antibody to human rhinovirus 14 penetrates the receptor-binding canyon. Nature 383:350–354
Sorger PK, Stockley PG, Harrison SC (1986) Structure and assembly of turnip crinkle virus. II. Mechanism of reassembly in vitro. J Mol Biol 191:639–658
Stehle T, Gamblin SJ, Yan Y, Harrison SC (1996) The structure of simian virus 40 refined at 3.1 A resolution. Structure 4:165–182
Stewart PL, Burnett RM, Cyrklaff M, Fuller SD (1991) Image reconstruction reveals the complex molecular organization of adenovirus. Cell 67:145–154
Stewart PL, Chiu CY, Huang S, Muir T, Zhao Y, Chait B et al (1997) Cryo-EM visualization of an exposed RGD epitope on adenovirus that escapes antibody neutralization. EMBO J 16:1189–1198
Stubbs G (1999) Tobacco mosaic virus particle structure and the initiation of disassembly. Philos Trans R Soc Lond B Biol Sci 354:551–557
Tao Y, Olson NH, Xu W, Anderson DL, Rossmann MG, Baker TS (1998) Assembly of a tailed bacterial virus and its genome release studied in three dimensions. Cell 95:431–437
Thuman-Commike PA, Greene B, Jakana J, Prasad BV, King J, Prevelige PE Jr et al (1996) Three-dimensional structure of scaffolding-containing phage p22 procapsids by electron cryo-microscopy. J Mol Biol 260:85–98
Thuman-Commike PA, Greene B, Malinski JA, King J, Chiu W (1998) Role of the scaffolding protein in P22 procapsid size determination suggested by T = 4 and T = 7 procapsid structures. Biophys J 74:559–568
Tsuruta H, Reddy VS, Wikoff WR, Johnson JE (1998) Imaging RNA and dynamic protein segments with low-resolution virus crystallography: experimental design, data processing and implications of electron density maps. J Mol Biol 284:1439–1452
Tuma R, Thomas GJ Jr (1997) Mechanisms of virus assembly probed by Raman spectroscopy: the icosahedral bacteriophage P22. Biophys Chem 68:17–31
van Raaij MJ, Mitraki A, Lavigne G, Cusack S (1999) A triple beta-spiral in the adenovirus fibre shaft reveals a new structural motif for a fibrous protein. Nature 401:935–938
Varghese JN, Laver WG, Colman PM (1983) Structure of the influenza virus glycoprotein antigen neuraminidase at 2.9 A resolution. Nature 303:35–40
Voss JE, Vaney MC, Duquerroy S, Vonrhein C, Girard-Blanc C, Crublet E et al (2010) Glycoprotein organization of Chikungunya virus particles revealed by X-ray crystallography. Nature 468:709–712
Wikoff WR, Johnson JE (1999) Virus assembly: imaging a molecular machine. Curr Biol 9:R296–R300
Wikoff WR, Liljas L, Duda RL, Tsuruta H, Hendrix RW, Johnson JE (2000) Topologically linked protein rings in the bacteriophage HK97 capsid. Science 289:2129–2133

Wikoff WR, Conway JF, Tang J, Lee KK, Gan L, Cheng N et al (2006) Time-resolved molecular dynamics of bacteriophage HK97 capsid maturation interpreted by electron cryo-microscopy and X-ray crystallography. J Struct Biol 153:300–306

Wildy P, Horne RW (1963) Structure of animal virus particles. Prog Med Virol 5:1–42

Wilson IA, Skehel JJ, Wiley DC (1981) Structure of the haemagglutinin membrane glycoprotein of influenza virus at 3 A resolution. Nature 289:366–373

Wolf M, Garcea RL, Grigorieff N, Harrison SC (2010) Subunit interactions in bovine papillomavirus. Proc Natl Acad Sci USA 107:6298–6303

Wynne SA, Crowther RA, Leslie AG (1999) The crystal structure of the human hepatitis B virus capsid. Mol Cell 3:771–780

Xu Y, Liu Y, Lou Z, Qin L, Li X, Bai Z et al (2004) Structural basis for coronavirus-mediated membrane fusion. Crystal structure of mouse hepatitis virus spike protein fusion core. J Biol Chem 279:30514–30522

Xu X, Zhu X, Dwek RA, Stevens J, Wilson IA (2008) Structural characterization of the 1918 influenza virus H1N1 neuraminidase. J Virol 82:10493–10501

Yu IM, Zhang W, Holdaway HA, Li L, Kostyuchenko VA, Chipman PR et al (2008a) Structure of the immature dengue virus at low pH primes proteolytic maturation. Science 319:1834–1837

Yu X, Jin L, Zhou ZH (2008b) 3.88 A structure of cytoplasmic polyhedrosis virus by cryo-electron microscopy. Nature 453:415–419

Zhang R, Hryc CF, Cong Y, Liu X, Jakana J, Gorchkov R, et al (2011) Cryo-EM structure of an enveloped alphavirus venezuelan equine encephalitis virus. submitted for publication. EMBO J 30:3854–3863

Zhang W, Mukhopadhyay S, Pletnev SV, Baker TS, Kuhn RJ, Rossmann MG (2002) Placement of the structural proteins in Sindbis virus. J Virol 76:11645–11658

Zhang X, Walker SB, Chipman PR, Nibert ML, Baker TS (2003) Reovirus polymerase lambda 3 localized by cryo-electron microscopy of virions at a resolution of 7.6 A. Nat Struct Biol 10:1011–1018

Zhang Y, Kaufmann B, Chipman PR, Kuhn RJ, Rossmann MG (2007) Structure of immature West Nile virus. J Virol 81:6141–6145

Zhou ZH, Prasad BV, Jakana J, Rixon FJ, Chiu W (1994) Protein subunit structures in the herpes simplex virus A-capsid determined from 400 kV spot-scan electron cryomicroscopy. J Mol Biol 242:456–469

Zhou ZH, Dougherty M, Jakana J, He J, Rixon FJ, Chiu W (2000) Seeing the herpesvirus capsid at 8.5 A. Science 288:877–880

Zimmern D (1976) The region of tobacco mosaic virus RNA involved in the nucleation of assembly. Philos Trans R Soc Lond B Biol Sci 276:189–204

Zubieta C, Schoehn G, Chroboczek J, Cusack S (2005) The structure of the human adenovirus 2 penton. Mol Cell 17:121–135

http://www.springer.com/978-1-4614-0979-3

Viral Molecular Machines
Rossmann, M.G.; Rao, V.B. (Eds.)
2012, XIV, 687 p. 221 illus., 192 illus. in color.,
Hardcover
ISBN: 978-1-4614-0979-3